MODEL ROCKETRY

November 1968
35¢

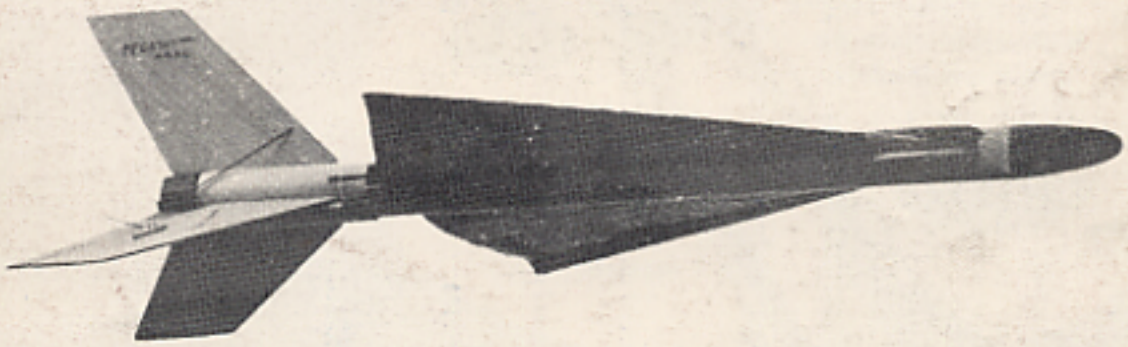

XR-5C: 3 STAGE CLUSTER

DRAG CALCULATIONS

VERSITEX PAYLOADER

SCALE: MT 135

AERIAL PHOTOGRAPHY

DYNAMIC STABILITY

FLEXWING RECOVERY

MODEL ROCKETRY

Volume I, No. 2

November 1968

XR-5C 2

Project Apollo 5

Technical Notes 7

Model Rocket Recovery by Extensible Flexwing 8

Scale: MT-135 15

Calculating Drag Coefficients 18

Questions and Answers 18

Versitex 19

NFPA Adopts Model Rocket Code 22

High Quality Aerial Photography 23

Fundamentals of Dynamic Stability 25

Club Notes 32

From the Editor

In recent years the existence of several major hobbies has been seriously jeapordized by the failure of the membership to attract new, young participants into the hobby. These hobbies have been forced to undertake large-scale recruiting programs in order to stir up interest.

In model rocketry we have not had this problem. The increasing membership roll of the NAR demonstrates that new people are continually joining our hobby. Model rocketry, however, faces an even greater crisis – the failure to keep older members interested in the hobby. The thrill of manning a launch panel and sending your own rocket into the sky, by itself, soon wears off. Over 950 of the first 1000 members of the NAR have left model rocketry in the past ten years.

The inability of model rocketry to retain experienced hobbyists seriously hinders the growth of the hobby. More programs and events such as the Research and Development competition in NAR sanctioned meets are needed to allow these older members greater opportunity for development and self-expression. The opportunities for research in such fields as low-speed aerodynamics, micrometeorology, photoreconnaisance, gasdynamics, rigid-body dynamics and exterior ballistics generated by the existence of model rocketry are virtually limitless. It is the responsibility of the Association, and of model rocketry in general, to take advantage of these potentialities.

Model Rocketry Magazine is published monthly by Model Rocketry, Box 214, Boston, Mass. 02123, at Central Sq. Cambridge, Mass. 02139.

Subscription rates: In U. S. and Canada, 1 year $3.50; Six months $2.00; single copy 35¢. Foreign, 1 year $6.00; Six months $3.50; single copy 60¢.

Material submitted for publication should be accompanied by self-addressed envelope if return is desired. We can assume no responsibility for material lost or damaged, but care will be exercised in handling.

Advertisers should contact Advertising Manager, Model Rocketry, Box 214, Boston, Mass. 02123.

Application to mail at second-class postage rates is pending at Central Sq. P.O., Cambridge, Mass. 02139.

XR-5C

MULTI-STAGE CLUSTERED ROCKET

Bill Luken

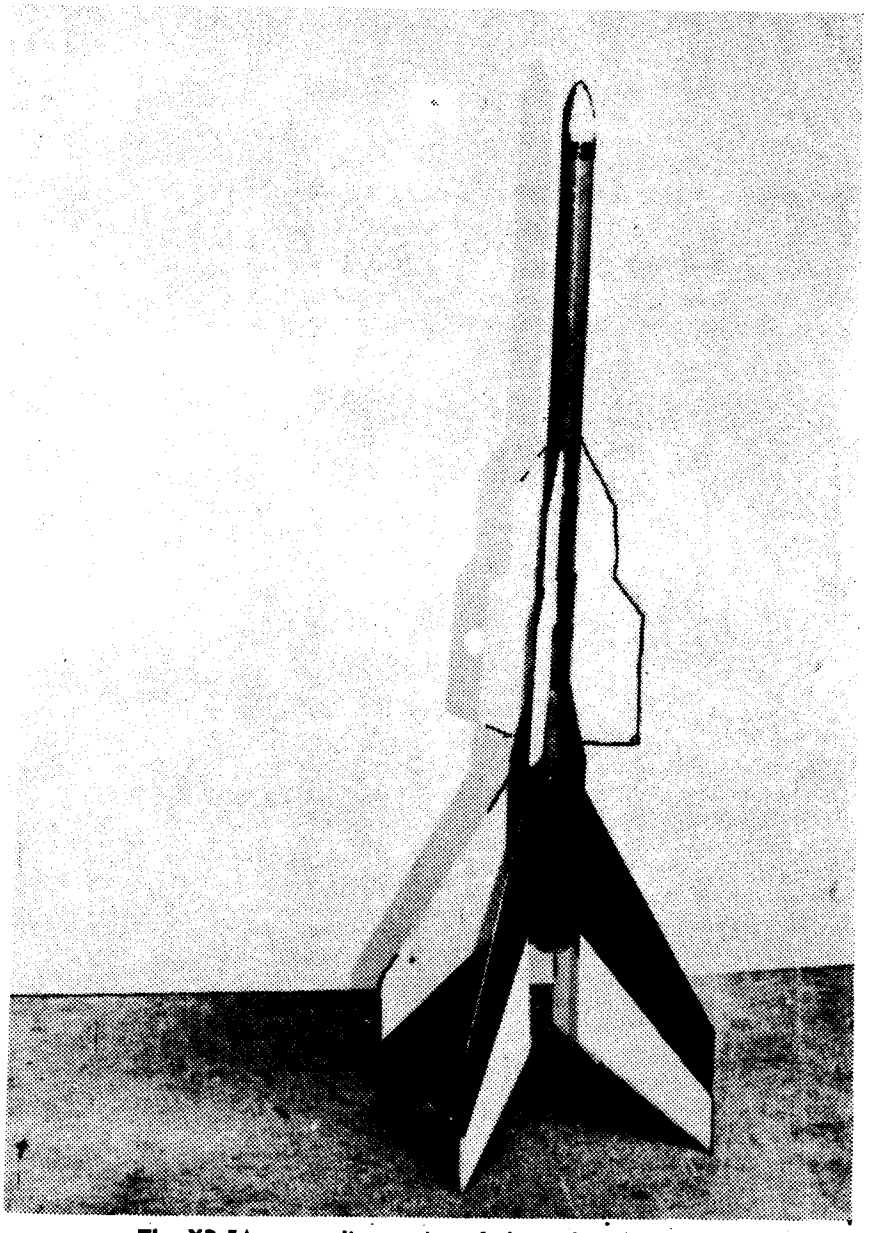

The XR-5A, an earlier version of the rocket described here. The XR-5C is essentially the same externally.

The "XR-5C" is a three-stage rocket which combines the high altitude abilities of multi-staging with the weight lifting abilities of clustering. This enables one to send an upper stage which is very large compared to the light-weight style high-altitude rockets to very high altitudes, while remaining within a restricted range of engines. The XR-5C was designed for use with B and C class engines. With minor modification the same design could be used to obtain high performance from the recently available C, D, and D engines. The design presented here is the end result of a development program aimed at building a rocket which could reach high altitudes without the recovery and payload restrictions of the light-weight style rockets.

In designing a rocket such as this, all of the design considerations of both clustered rockets and multi-staged rockets must be taken into account. Some of the major problems are:

I. The concentration of weight in the cluster of engines tends to make the rocket tail-heavy, decreasing the stability of the rocket.

II. The concentration of weight in the tail moves the center of gravity so far back that both the second and the third stages are ahead of the center of gravity. Both upper stages require fins for their own stability, but since these fins are all ahead of the center of gravity of the assembled rocket, they decrease the stability of the total design.

III. The junction between the second stage and the booster must be designed to give a streamlined transition between the body tube sizes involved, to hold the second stage in a steady vertical position, and, at the same time, allow for reliable ignition of the second stage.

The first step in investigating the design considerations needed to overcome these difficulties was the design of a prototype, the XR-3. The XR-3 was a two stage rocket using a three engine cluster for a booster, and a single engine upper stage. One model, the XR-3C, is shown in an accompanying photograph. The XR-3C required very large fins to overcome problems I and II. Even so, tests showed that a critical period occurs just after the rocket clears the end of the launch rod. The rocket is accelerating, and at this time it is just going fast enough to be stable, but it is very sensitive, and it may cant a bit before gaining enough speed to be steady. Some control was gained by setting the booster fins at an angle to spin the rocket. Even with the spin fins, though, it is recommended that an extra long launch rod (54") be used in place of the regular 36" rod.

In order to reduce the instability caused by the upper stage fins (problem II), the upper stage fins are located as far back on the body as possible, and they are designed to fit flush against the tapered adapter section. This design minimizes the drag moment of the torque caused by the fins by bring-

XR-5C

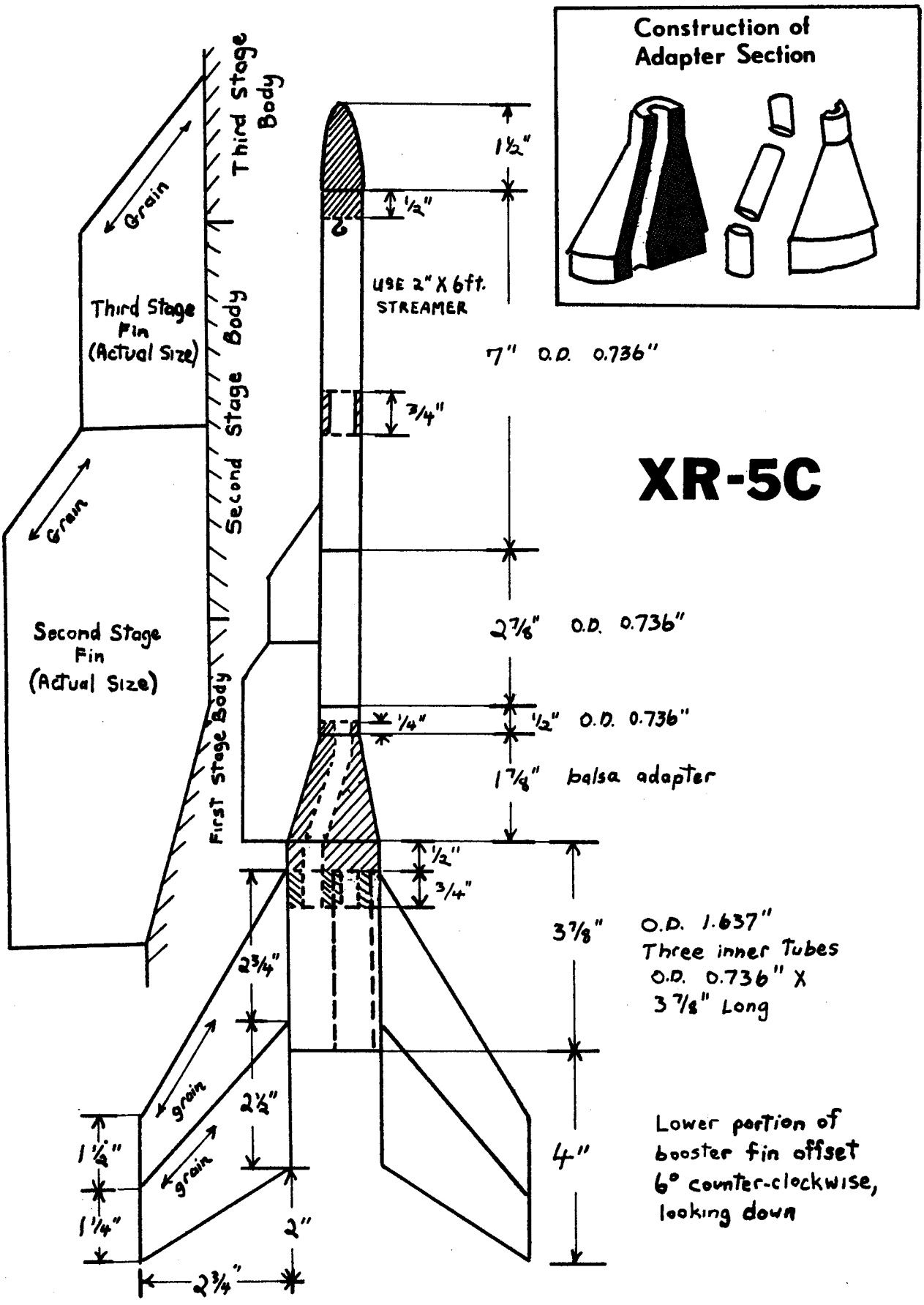
Construction of Adapter Section
Third Stage Body
Grain
Third Stage Fin (Actual Size)
Second Stage Body
Grain
Second Stage Fin (Actual Size)
First Stage Body
1½"
½"
USE 2" X 6ft. STREAMER
7" O.D. 0.736"
¾"
2⅞" O.D. 0.736"
¼"
½" O.D. 0.736"
1⅞" balsa adapter
½"
¾"
3⅞"
O.D. 1.637"
Three inner Tubes
O.D. 0.736" X
3⅞" Long
2¾"
grain
2½"
grain
1¼"
1¼"
2"
2¾"
4"
Lower portion of booster fin offset 6° counter-clockwise, looking down

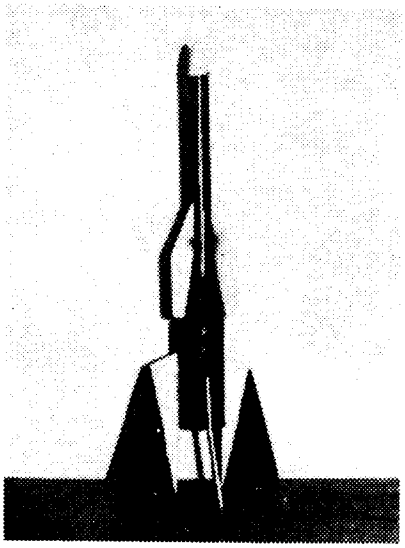

The XR-3C prototype. This rocket has a cluster of three engines in the booster and a single engine in the upper stage.

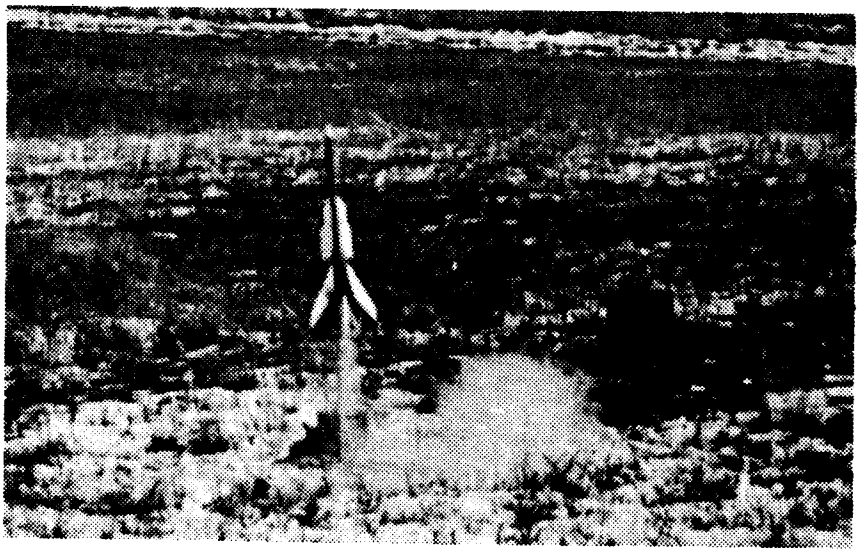

The first launch of the XR-5A. Note the unbalanced thrust (the white area beneath the booster). Only one engine had ignited.

ing them as close to the center of gravity as possible. Making the fins flush against the adapter also reduces the drag by cutting down on trailing edge area. This also ensures firm vertical orientation of the second stage without restraining its freedom to separate during staging.

In all models of the XR-3 and the XR-5, streamer type recovery was used. This was done because this type of recovery gives maximum visibility to the returning rocket. The streamers used are one inch wide and six feet long, made of tightly rolled red crepe paper.

For the XR-5, the booster fins were redesigned, made larger, and increased in number from three to four. This was done to compensate for the increased fin area of the upper stages (larger problem II effects). The fins of the upper stages were made to fit together in an integrated design to reduce the leading and trailing edge area. They were made as small as possible, but they were restricted by the fact that the third stage fins must attach to the third stage and the second stage fins must be large enough to stabilize the combined upper stages. As with the XR-3, the second stage fins were made to fit flush against the adapter section.

The XR-5A employed a more complicated stage coupling scheme between the first and second stages than the design shown here. This was also used on the XR-3 series, but it was finally dropped as unnecessary and ineffective.

An important change was made in the XR-5C model. All previous models used a hollowed out balsa adapter section which gave all three booster engines access to the second stage engine. Thus, any of the three booster engines could ignite the second stage engine, virtually ensuring that the second stage engine would ignite. This was found to be a great disadvantage when one or two of the booster engines would fail to ignite. In that event, the remaining en-

(Continued on page 31)

Another catastrophe. The second stage fired nearly horizontal and the third stage went into a power-dive, hitting the ground roughly 1000 feet from the launch site. The second stage was not recovered.

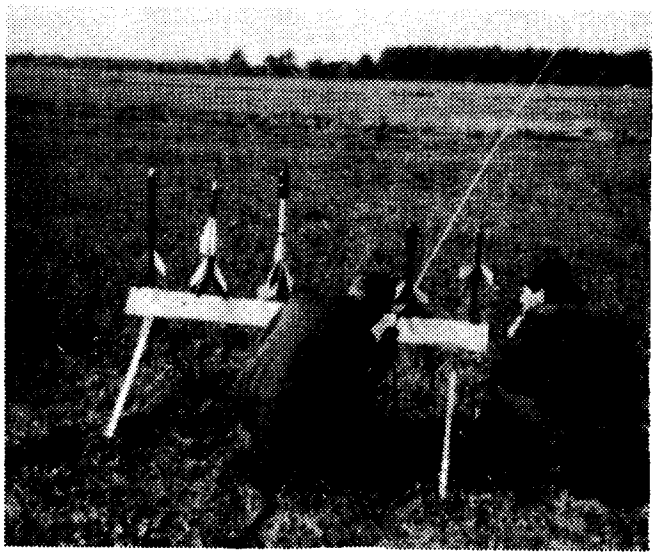

The XR-5B ready for take-off at an M.I.T. launch.

Project Apollo

George Flynn

(Kennedy Space Center, Fla. Oct. 12, 1968) Last month's near perfect launching of the Apollo 7 spacecraft from Cape Kennedy was a significant step in the American effort to land a man on the moon in this decade. The success of this planned 10 day 21 hour mission has boosted the hopes of NASA officials that the first American lunar landing will come in the fall of 1969. The successful flight of Apollo 7 has assured the assignment of a more ambitious mission to the Apollo 7, which will be launched by a Saturn 5 vehicle in mid-December.

This Saturn 5 booster, which was rolled out of the Vehicle Assembly Building last week and is now undergoing a two month final checkout at the launch site, was originally slated to carry an unmanned spacecraft into orbit in a duplicate of last April's Apollo-Saturn 502 mission. However, following the flight of AS-502, the Saturn 5 booster was man-rated after only two unmanned flights. A new spacecraft was checked out and mated to the Saturn 5.

Apollo 8 was scheduled to be a long-duration earth-orbital flight designed to test the Apollo systems. However, two alternative mission profiles are now under consideration. The most ambitious of these would have the Apollo 8 orbit the earth twice while the performance of the onboard systems is evaluated. Then the spacecraft would be injected into a "free return" lunar trajectory. As the spacecraft neared the moon a Service Propulsion System engine burn would inject the Apollo 8 into lunar orbit. Apollo 8 would orbit the moon 10 times before returning to earth. Since there will be no Lunar Module on the Apollo 8 mission, there can be no lunar landing on this flight.

Ed. Note: This report, written at Cape Kennedy shortly after witnessing the launching of Apollo 7, is the first in a series of articles detailing the progress of the space effort. In future issues, Model Rocketry reporters on the scene at major space events will keep readers informed of new developments on the aerospace horizon.

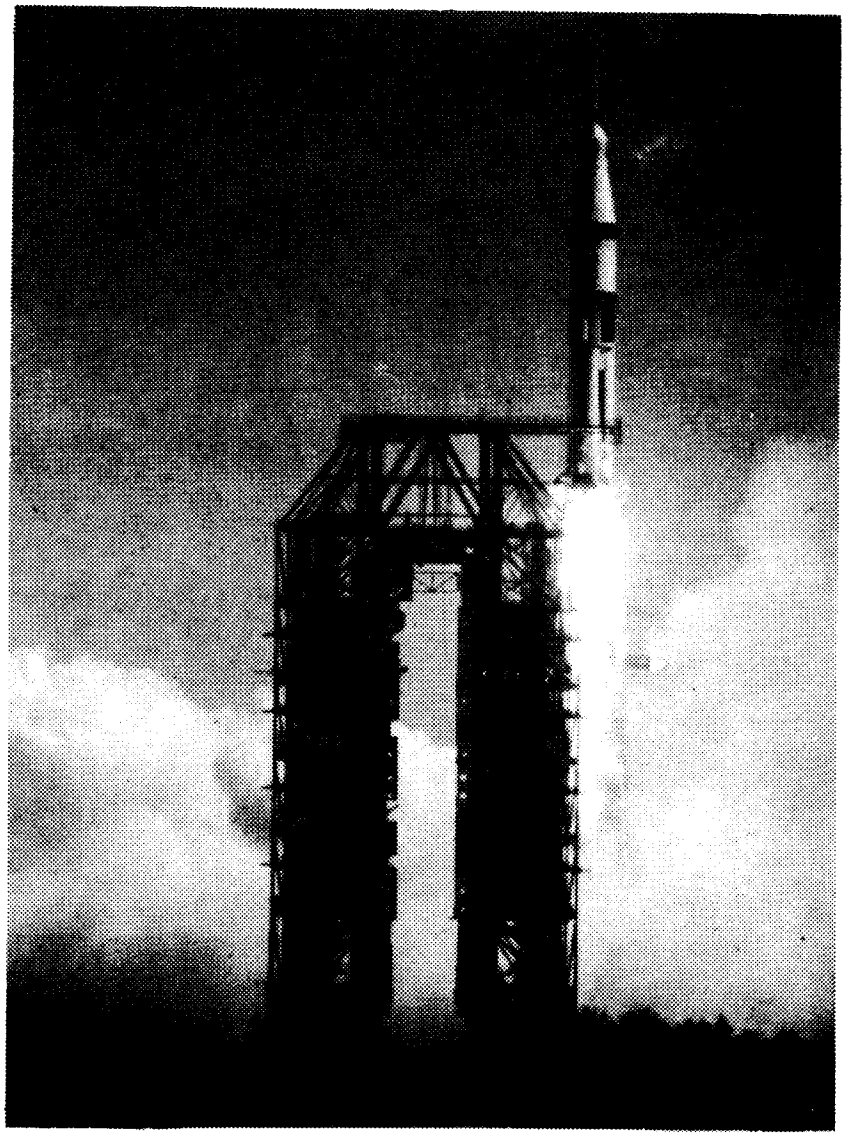

Photo by George Flynn

Apollo 7 Lift-off

The second Apollo 8 mission alternative is to fly a "free return" lunar trajectory and return to earth without orbiting the moon. In the case of an earth orbital flight, if trouble develops in any of the onboard systems, an emergency return to earth is possible within about 20 minutes. However, once committed to a lunar trajectory, this

emergency recall capability is lost – the spacecraft is committed to remain in space for about 5 days. Thus trouble with any critical system, such as the life support system, on the Apollo 7 flight would have caused rejection of the alternate Apollo 8 plans. However the excellent performance of all critical subsystems on Apollo 7 makes possible a lunar Apollo 8 mission.

The Apollo 9 mission will be the first test of the Lunar Module. This flight will be confined to an earth orbital mission on the rendezvous and docking maneuvers necessary to the lunar flight will be practiced. Apollo 10, which should be flown in early May of next year; is presently scheduled to be a repeat of the Apollo 9 flight. However, a success on the Apollo 9 might cause NASA officials to reconsider the flight plan, as is being done with Apollo 8. Thus the Apollo 10 astronauts could fly a lunar landing mission.

As the program presently stands, Apollo 11 and 12 are schedule to be "free-return" lunar flights, with the possibility of lunar orbit and then lunar landing to be decided as the missions progress. Though the exact timetable is highly dependent on the success of all previous flights, the first American landing on the moon should come by the fall of 1969.

As our own plans for a manned lunar landing are being accelerated, the Russians are not inactive in this field either. According to Wernher von Braun, the official view is that the Zond 5 spacecraft, which was recently recovered after a "free return" lunar mission, was in fact an unmanned version of the Soyuez manned spacecraft. The flight profile for the Zond 5 mission indicates that it was a low deceleration reentry attempt. If the flight was designed only to recover instrumentation, a high deceleration (50 or 60 g's) reentry profile could have been flown. Such a flight path assures easier recovery, but it was not chosen according to von Braun because "This was a dress rehearsal for a manned flight. They went through all this trouble in order to demonstrate to themselves that they can fly a reentry flight path with occupants where the deceleration would not have exceeded the limits cosmonauts could have tolerated."

Since ground testing on the new Russian booster rocket, which is thought to have 10 million pounds of thrust (about 1-1/3 times that of the Saturn 5), is nearly complete, this rocket could be used in the Russian lunar landing program. Von Braun speculated that the lack of serious Russian interest in rendezvous and docking (though they have twice docked Cosmos satellities by ground command) does not indicate a lag in the Russian program, but only they they do not intend to use orbital rendezvous and docking in their first manned lunar landing.

The Russians may have adopted a lunar landing mission profile similar to one originally considered by the United States. An unmanned vehicle containing all the necessary propellant and supplies for a lunar return mission would first be soft-landed on the moon. The condition of the payload would be extablished by radio data. Then a manned spacecraft would be flown to the same area on the lunar surface, and the cosmonauts would return to earth using the supplies carried by the first vehicle. Such a mission profile would be typical of the "brute force" method characteristic of the Russian space program. If the new Russian booster is subjected to two unmanned flight tests prior to man-rating, von Braun suggests that the Russians could land a man on the moon by the summer of 1969. Thus next year promises to be highly significant in both the American and Russian manned lunar programs.

TECHNICAL NOTES

GEORGE CAPORASO

One of the most talked about subjects in model rocketry over the past few years has been that of altitude prediction. Having been begun with crude, lengthy calculating procedures the problem is now nearing a satisfactory solution.

What is a satisfactory solution? To answer that we must briefly explain the flight behavior of a typical rocket. The engine of a typical model rocket will burn for about a second, during which about 20% of the rocket's total altitude will be reached. After burnout, the rocket decelerates rapidly and coasts for about 5 seconds after which the recovery system is deployed. During the ascent phase, the rocket may have experienced oscillations due to winds, misaligned fins, etc. The satisfactory solution of the altitude problem must take into account the effect of drag and oscillations on the rocket.

To the author's knowledge, the first attempt to include the effect of drag on the performance of model rockets appeared in an ancient Estes Industries Model Rocket News under the heading "Rocket Math." It consisted of a rather lengthy and involved set of repeated calculations but gave a fairly accurate answer for most rockets provided the drag characteristics of the rockets were known. Unfortunately, no theoretical method for calculating them was known by modelers at that time.

A breakthrough was made in late 1964 when Len Fehskens, 1964 NARAM leader team champion, derived a relatively simple approximation to the altitude problem which gave the exact answers that the previous Estes procedures gave only approximately. Unfortunately, Fehskens did not publish his work. However, as is almost always the case, someone somewhere else was working on exactly the same problem and in 1965-1966, the same solutions were obtained independently by Douglas J. Malewicki of Estes Industries. These results were published in a fine technical report by that company. At roughly the same time, the author obtained different solutions to the problem and published them . The author then modified both the Fehskens-Malewicki solutions and his own solutions to account for the change in the rocket's weight with time during the burning of the engines, thus extending the usefulness of the solutions to rockets where the fuel comprises a substantial amount of the rocket's weight .

Recalling that frantic period where we all lived by the "publish or perish" rule, I can only laugh at the collective ignorance of model rocketeers (myself included) who never stopped to think that such problems might have been solved before and that the answers might be sitting around in a book on some dusty library shelf. Well, they were. Take a look at "The Exterior Ballistics of Rockets" by Davis, Follin and Blitzer, published in 1958 by Van Nostrand, and you will see lying on pages 86 and 87 the Fehskens-Malewicki solutions. The biggest surprise comes when you discover that the coasted time and coasted altitude equations were first derived by Bernoulli long before model rocketry ever existed!

Nevertheless, some of our altitude approximations and corrections had never been obtained previously and did constitute a contribution to the field. Also, the range of a rocket launched at any angle was obtained .

However, two problems still remained. First, how does one figure out his rocket's drag coefficient without actually testing for it after building his rocket and secondly, how does one couple the oscillations of a rocket to the altitude?

As usual, the answers already existed in aerodynamics books . However, the problem was finally resolved for model rocketry when Prof. J. Gregorek of Ohio State University submitted a paper to the NAR on calculating drag coefficients. His paper provided a compact method of predicting the drag characteristics of model rockets without the necessity of building and testing them. An alternate method is presented elsewhere in this issue.

One problem now remains; that of figuring the effect oscillations have on the altitude of model rockets.

Gordon Mandell's classic treatment of the dynamic stability of fin stabilized rockets now brings this last problem closer to a solution. The author is presently working on this problem and has had some encouraging success. He hopes to present this last phase of the problem and its solution in an issue of Model Rocketry in the near future.

1. "Calculating Model Rocket Performance" by G. J. Caporaso from TECH ENGINEERING NEWS, Oct., 1967.
2. "Solutions of the Differential Equations of Ballistic Flight Paths for Model Rockets" by G. J. Caporaso, a paper presented to the 1968 M.I.T. Model Rocketry Convention.
3. "The Exterior Ballistics of Rockets" by Davis, Follin and Blitzer. 1958 by D. Van Nostrand Co. pages 50-54.
4. "The Linearized Rotational Dynamics of Streamlined Projectiles" by G. K. Mandell, a paper presented to the M.I.T. Model Rocketry Convention, 1968.

Coming Next Month

Avenger II: Class F Altitude

Constructing a Launch Panel

Dynamics: Part III

Using Super Monokote

Viking IV Scale

Design Studies in

Model Rocket Recovery by Extensible Flexwing

Gordon K. Mandell

In accordance with Federal and Association regulations, all non-professional rocket vehicles of the model classification are required to incorporate systems for providing a controlled descent and soft landing, that the vehicle structure shall present no hazard to personnel or property and that the model shall be capable, as is an air craft, of repeated flights. In the decade since the founding of the National Association of Rockety, numerous techniques for the safe recovery of model rockets have been developed. Parachutes, drag streamers, and dive-braking systems of various descriptions have all been tested and found satisfactory within given ranges of applications. All, however, have obvious limitations: parachutes suffer from a lack of directional control only slightly alleviated by automatic shroud-adjusting and reefing techniques, while the other systems are acceptable only on the lightest models. The most recently developed recovery systems, and among the most promising, are those of the "boost-glide" family, a generic term applied to all techniques whereby the vehicle completes the descent phase of its flight in a configuration of aerodynamic characteristics permitting a controlled glide. In free flight, of course, one faces the same drift and loss probabilities as with parachutes, but the potential controllability of the boost-glider is much greater, and with the installation of a radio-command guidance system of the type used in model aviation the probability of recovery may be greatly increased.

The boost-gliders comprise numerous types; all, however, fall into three basic categories: rear-engined, forward-engined, and flexwing. These major groupings and the design spectra contained there in are illustrated in Figure 1. Researches too numerous and extensive to enumerate here relating to structural and aerodynamic design criteria for the various versions have been carried out by interested individuals. The subject of this discussion will hereafter be restricted specifically to the *extensible flexwing*, whose design the author has investigated in some detail.

Mission Requirements and Vehicle Characteristics

The extensible flexwing was developed in order to perform a mission basically different from that of most of its rigid-winged counterparts. Almost since their inception, the major application of boost-glide vehicles in model rocketry has been in sporting activity: competition among designs in which the overall vehicle efficiency is indicated by the greatest flight time attainable, analogous to duration competition among glider pilots and model aviators. While some varieties of flexwing have successfully entered such competition, duration was not intended as an objective of the extensible flexwing; its purpose, rather, was to combine the ground support, handling, and flight characteristics during boost of the finstabilized ballistic rocket with the flight characteristics of a conventional aircraft in descent. Large, fragile surfaces and their attendant difficulties due to acceleration and aerodynamic loads were to be eliminated during the early stages of flight. The absence of such surfaces would also preclude the likelehood of a highly erratic flight path in the presence of wind gradients. The mechanism for actuating the recovery system would have to conform to the usual requirements for strength and simplicity of moving parts for ease of, or elimination of the need for, maintenance and repair in order to insure high long-time reliability and field readiness. Glide-phase requirements included deployed surfaces of sufficient area to assure an acceptable rate of descent, an adequate vehicle lift/drag ratio, and the inherent stability necessary to all free-flying aeromodels. To these was added the specification that the vehicle possess sufficient internal volume for the installation of miniaturized equipment of various types, as well as the center-of-gravity range tolerance and wing area to sustain the added load. The present extensible flexwing design has been specifically developed to fulfill these mission criteria in their entirety.

Formulation of the Basic Design

The injunction against extended surfaces in boost immediately removed all rigid-winged configurations except the variable geometry from consideration. The variable-geometry vehicle, moreover, retains the whole of its wing area exposed to the airstream, simple shifting the area distribution closer to the body centerline during rocket flight. This is, of course, desirable from a structural and drag standpoint, but it was felt that greater gains might be made by going to a flexwing configuration.

The suspended flexwing (parawing, or Rogallo wing) had been built in several varieties previously, but had exhibited some severe handicaps in application to model-sized vehicles. Large hatches or clamshell doors had to be built into the body tubes to release the wings. Their shroud lines tangled more often than those of parachutes, and in glide phase, they were subject to severe aerodynamic effects arising from the oscillations of the suspended mass of the vehicle. Such pendulous oscillations often casued the "bellied" wings to spill wind, creating a feedback situation that soon collapsed the flexwings entirely. Certain versions expelled from the noses of models had met with some success, but these were somewhat self-defeating, since the major part of the rocket required another recovery system. It thus became apparent that a flexible plastic wing stored within the model, but extended directly

from its sides in a manner similar to the variable-geometry rigid wing, would offer a desirable combination of advantages and would stand an excellent chance of fulfilling the specified performance criteria. The development of today's extensible flexwing consists in the refinement of this basic concept.

The Experimental Construction and Flight Test Program

With a full-sized vehicle, of course, the basic design would have had to be refined by exhaustive tests and painstakingly detailed. With the miniaturized and simplified structures of models, however, it proved desirable to proceed directly to the construction and flight testing of prototypes in conjunction with the laboratory testing of components, rather than awaiting their completion. In all, eighteen experimental extensible flexwing models were built and test flown during the study, the rocket power being supplied by a selection of standard model propulsion units ranging in impulse from 0.35 to 1.15 pound-seconds.

It soon became evident that the flight test program would have to deal with two major problem areas: actuation and deployed configuration. The first five vehicles of the series were so seriously plagued by one or another of these difficulties that they never progressed beyond unpowered glide testing; powered flight would have been a waste of propellant. A workable design was finally arrived at in which a single mechanism restrained the wing in a fuselage sheath during boost and released it for glide with the expulsion of the expended engine casing. The wing itself was of paper-thin polyethylene and was sewn folded over its leading-edge booms, made of thin birch dowel. The booms were joined at their forward extremities by light sheet-aluminum flanges pivoted about a small machine screw; a "scissor spring" of music wire, concentric with the flange pivot, provided the torque for deployment. Implanted in the wingtip end of each boom was a small, offset, right-angled hook, also of music wire, which passed through a port in the vehicle afterbody and braced outward against the forward inside wall of the motor casing. With the engine in place the "retainer hooks" held the booms inboard; when the engine ejected free of the hooks the scissors assembly deployed the wing.

Once deployment problem was solved, the aerodynamic problem still remained.

The extended wing had little airfoil, as it did not belly greatly against the spring tension, and lift had to be obtained by inducing a positive angle of attack. This could be effected in two immediately apparent ways: by building root incidence into the wing and by using movable surfaces to induce positive pitch in the whole vehicle. The first of these techniques proved ineffective, as no more than three degrees of incidence could be built in without sacrificing much of the body volume peripheral to the wing sheath, and this amount was virtually "ironed out" by the slight belly of the wing a glide speed, resulting in a catastrophic nosedive.

Turning to the second technique, the most feasible position for a movable surface appeared to be the trailing edge of a fin,

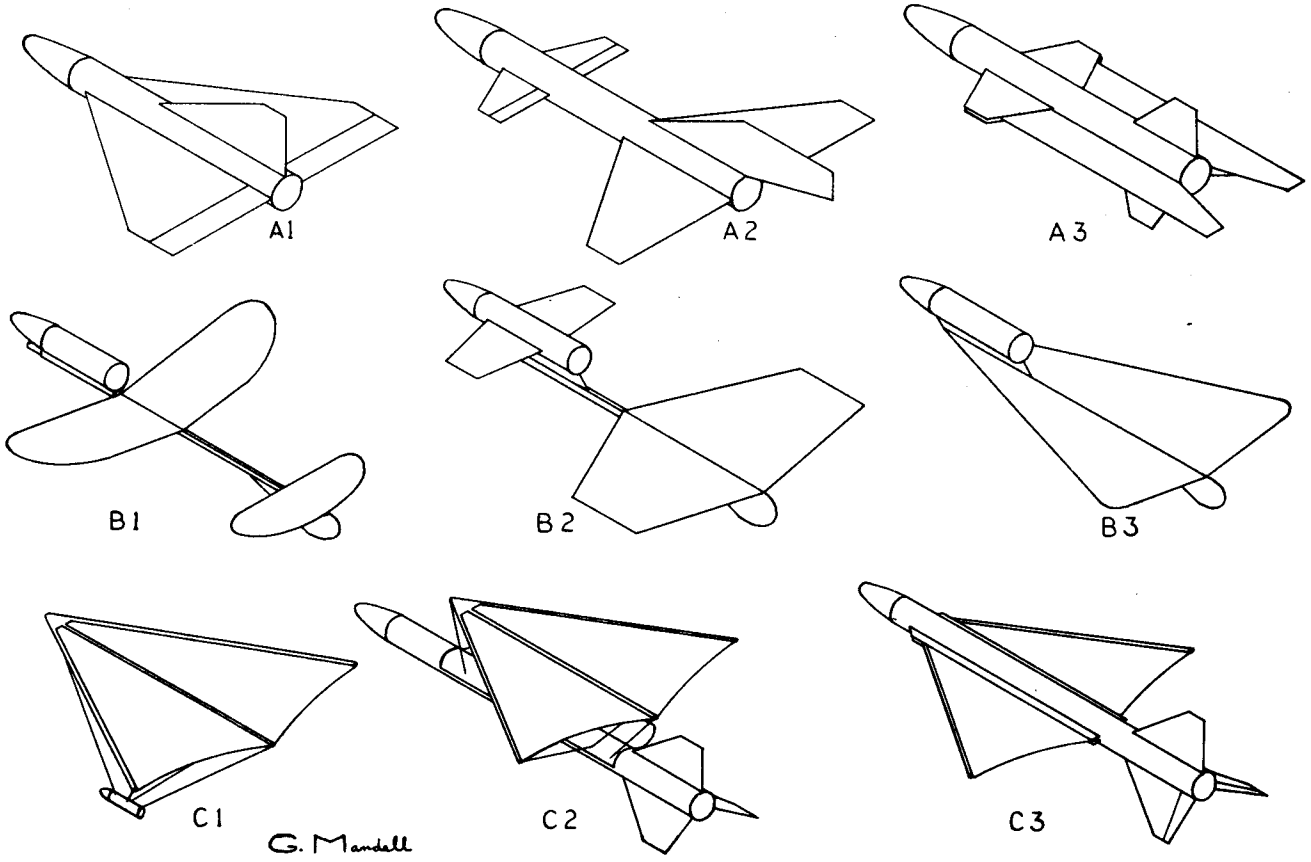

Figure 1. Representative types of Glide-Recoverable Model Rockets.

Row A: rigid wing, rear-engined
- A1: conventional (delta)
- A2: canard
- A3: variable geometry (shown in boost configuration)

Row B: rigid winged, forward-engined
- B1: conventional
- B2: canard
- B3: delta

Row C: flexwing (all shown in glide configuration)
- C1: suspended payload
- C2: full vehicle suspended
- C3: extensible flexwing

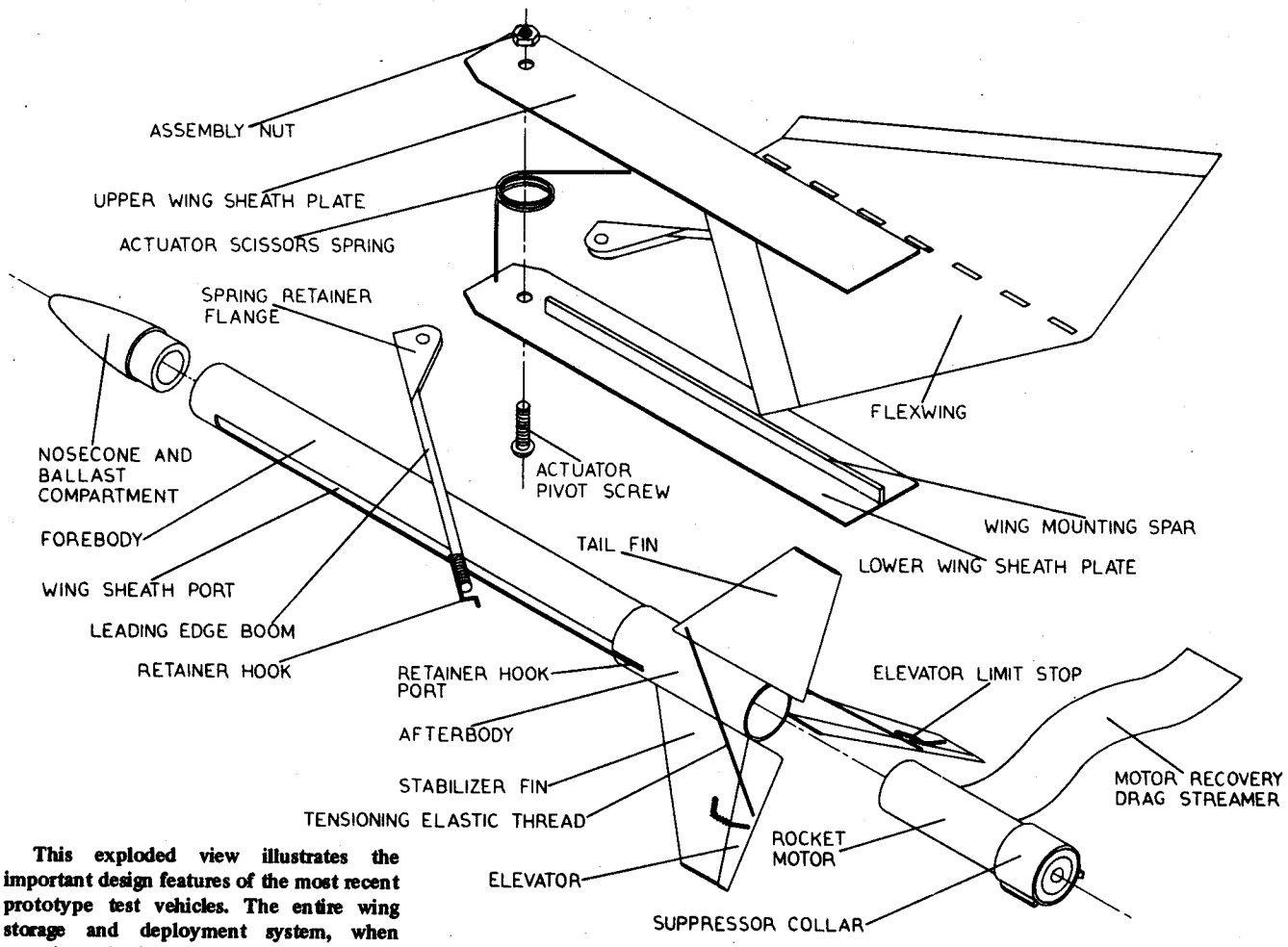

This exploded view illustrates the important design features of the most recent prototype test vehicles. The entire wing storage and deployment system, when complete, is installed through the wing sheath port. Sheath plates extend from forebody, forming a flange which allows the wing to be more neatly stowed in boost.

where it would function as an aircraft elevator, as this entailed the least extra structure and gave the cleanest configuration. A standard boost-glide actuating system was originally installed on the elevators: wire bars restrained by the after motor casing to hold a neutral setting in boost, elastic thread to provide elevating torque in glide. The bar system has subsequently been replaced by a "suppressor collar" mounted on the motor casing and incorporating rails to restrain the elevators during boost. At ejection, the collar/engine assembly is jettisoned and recovered by a drag streamer; the remainder of the vehicle, its elevators now operative and wing deployed, is glide-recovered.

The wide configurational tolerance of the prototype designs gave full opportunity for visual evaluation of the relative aerodynamic merits of individual designs via flight performance. Such data indicated that higher aspect-ratio flexwings with the concomitant lower vehicle fineness ratios,

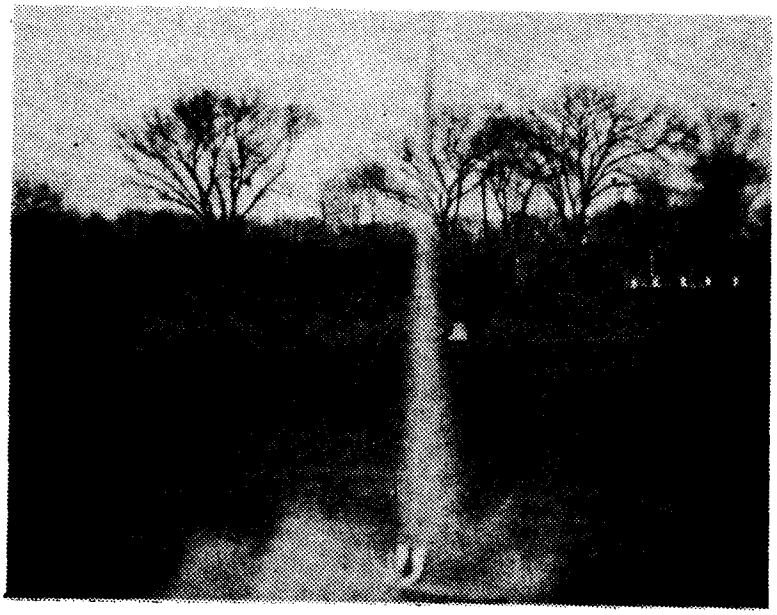

Figure 3. A prototype extensible flexwing vehicle lifts off in a successful powered flight test. At the instant of liftoff, balsa, polyethylene, and fiberboard vehicles must withstand accelerations approaching fifteen G.

and leading-edge sweep angles closer to 45 degrees than to 70 degrees gave the best all-around performance. More quantitative data than this, however, were not obtained by such crude methods and a rudimentary wind tunnel testing program was inagurated in hopes of obtaining finer definition between the configurations.

The Wind Tunnel Test Program

A complete professional program would necessarily include wing, body, fin, and complete vehicle data for lift, drag, yaw, pitch, roll, and side force. Limitations of time, personnel, and equipment, however, have precluded such a complete procedure to date and have limited the data thus far taken and completely reduced to the lift/drag performance of wing configurations and a few preliminary studies of body/fin assemblies.

The tunnel and balance system used is shown with explanatory notes in Figures 4 and 5. The wing planforms tested, illustrated in Figure 6 were of substantially identical structure to those incorporated in the flight prototypes. Each had an area of 36 square inches; all were tested at an airspeed of 20 feet per second to maintain dynamic similitude with respect to free prototype flight. The results of these model test are set forth in the airfoil characteristic graphs obtained therefrom (Tests No. 021 through No. 017) and provided with explanatory notes. While the fact that the test equipment was for the most part handmade tends to limit the accuracy (.0005 lb. in lift, .0004 lb. in drag, .005 inch H_2O in the velocity manometer), the system has performed quite well within its limitations and its data are considered generally reliable.

Interpretive Notes for Wind Tunnel Test Data

Facility: tunnel or laboratory where test was performed. WT-5.12 is the designation of the wind tunnel described.

std.: standard stmospheric pressure. The tunnel is located near sea level and is not sealed for pressurization to higher levels.

RN: Reynolds Number: a scaling factor used in establishing dynamic similitude in order to properly relate the test to actual flight. RN is defined as the ratio of inertial to viscous forces in a moving fluid medium and is computed from the relationship

$$RN=(P/\phi)VL$$

where P is the fluid density, ϕ the fluid viscosity, V the velocity and L the length of the object being tested.

C_L: Coefficient of lift; a dimensionless coefficient depending on the shape and RN of the object tested. In practice it is computed from the relationship

$$L=(P/2)C_L AV^2$$

where L is the lift generated by the object, A a standard cross-sectional area through the object (planform, in the case of wings), and V the velocity.

C_D: Coefficient of drag, analogous to C_L in meaning and computation.

L/D: Ratio of lift to drag, a common criterion of aerodynamic efficiency.

θ: angle of attack; the angle at which a line drawn through the leading and trailing edges of the mean aerodynamic chord meets the direction of the airstream. In these tests, mean aerodynamic chord was assigned as the longitudinal bisector (axis of bilateral symmetry) of the planform.

Data have been corrected as well as available techniques allow for tare, interference, and pitching moment effect on drag reading.

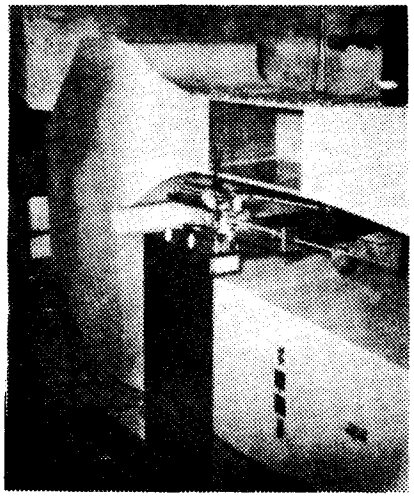

Figure 4. The wind tunnel and balance used in the laboratory test program. Tunnel is of galvanized sheet, plywood, and plexiglas and is powered by two electric drives totalling 2.3 horsepower. Speed of the airflow is infinitely variable from zero to maximum. Flow velocities to 55 feet per second have been produced in the 8-by-12-inch test section, which can accommodate models up to 22 inches in length, and 100 feet per second is a possibility with an uprated power source. The balance, mounted on a plywood table to insulate it from tunnel vibrations, is of stainless steel and aluminum, reads lift and drag on its single support arm, and has an electrically driven "fine" scale.

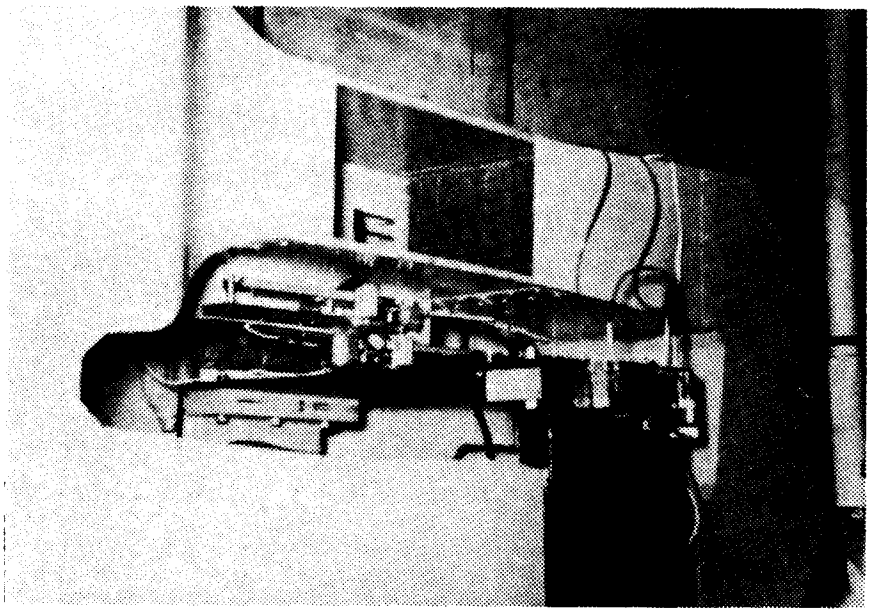

Figure 5. Another view of the tunnel/balance system, here with the balance installed and operative. Commercial draft gauge pressed into service as velocity indicating manometer has been mounted on the side of the balance table.

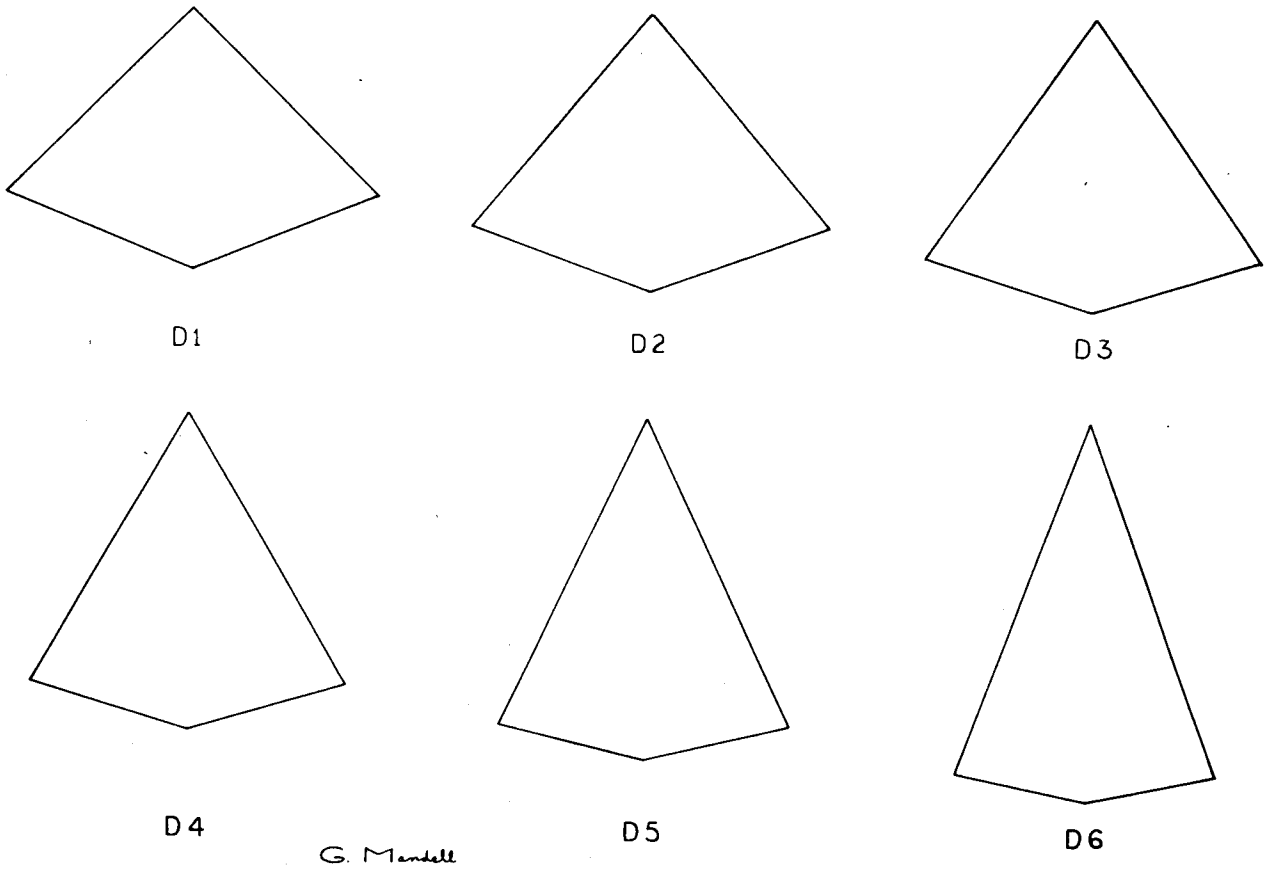

Figure 6. Planform Views of Wind Tunnel Test Wings. Wings were constructed of polyethylene and dowelling, as in flight models, that they might have similar characteristics of deformation under air loads. The only difference between wind tunnel and flight wings is that former have slightly greater area, are braced in permanently extended position.

The test results indicate no really major differences in the lift/ drag behavior with changing aspect ratio. This is understandable, as in still air the wings are virtually flat plates; they acquire what little airfoiling they possess by bellying under aerodynamic loads. Such bellying is slightest with the higher aspect ratio wings, greatest with the lower aspect ratios, as their long booms are rather easily elastically deformed. From the tunnel tests, the result appears to be that both lift and drag are somewhat reduced at the higher aspect ratios. Comparison of the L/D ratios, a common efficiency measurement, must be considered questionable due to the fact that drag near the angle-of-attack range associated with the L/D peak decreases to a level near the accuracy of the balance, as well as entering a region where tiny drag changes produce large changes in L/D. It is definitely significant, however, that in comparing the flexwings as a whole to a rigid flat plate at comparable Reynolds Numbers (Test No. 018), We find that the L/D ratios of the flexwings are some two to three times that of the plate. The aeroelasticity effects are evidently

Characteristic	Preferred	Acceptable	Unacceptable
root incidence	none, with elevators	slight positive, with elevators	any, without elevators
wing storage mode	flanged sheath	vertical center brace with side longgerons	non-flanged sheath, rotary breech, longitudinal hatch
engine recovery mode	braked module		free
elevator suppressor mechanism	suppressor collar on engine casing	internal suppressor bar	
wing deployment mode	extensible, spring-loaded scissors actuation		suspended
fin placement	triform	no data to date on cruciform	

Figure 7. Qualitative design criteria for extensible flexwing rocket vehicles.

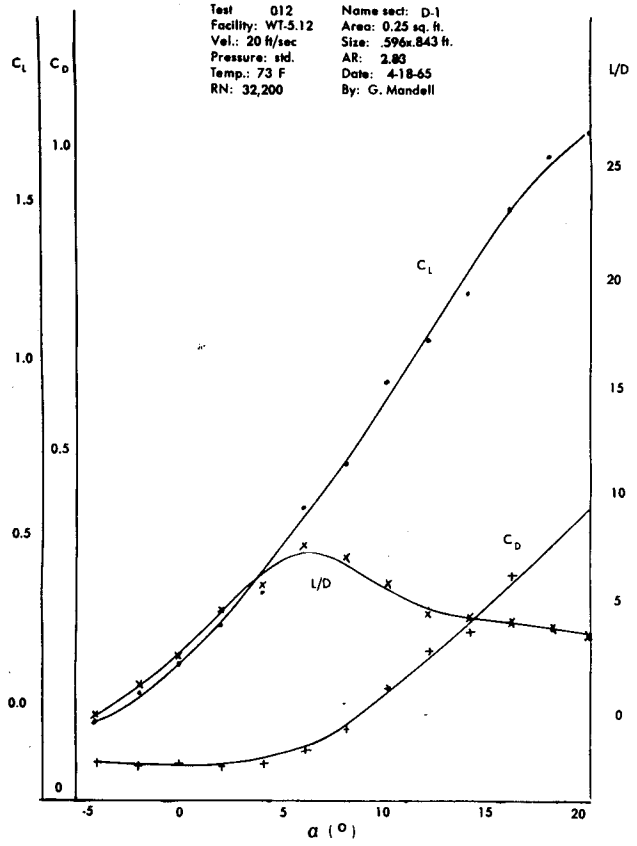
Test 012
Facility: WT-5.12
Vel.: 20 ft/sec
Pressure: std.
Temp.: 73 F
RN: 32,200
Name sect: D-1
Area: 0.25 sq. ft.
Size: .596x.843 ft.
AR: 2.83
Date: 4-18-65
By: G. Mandell
C_L
C_D
L/D
α (°)

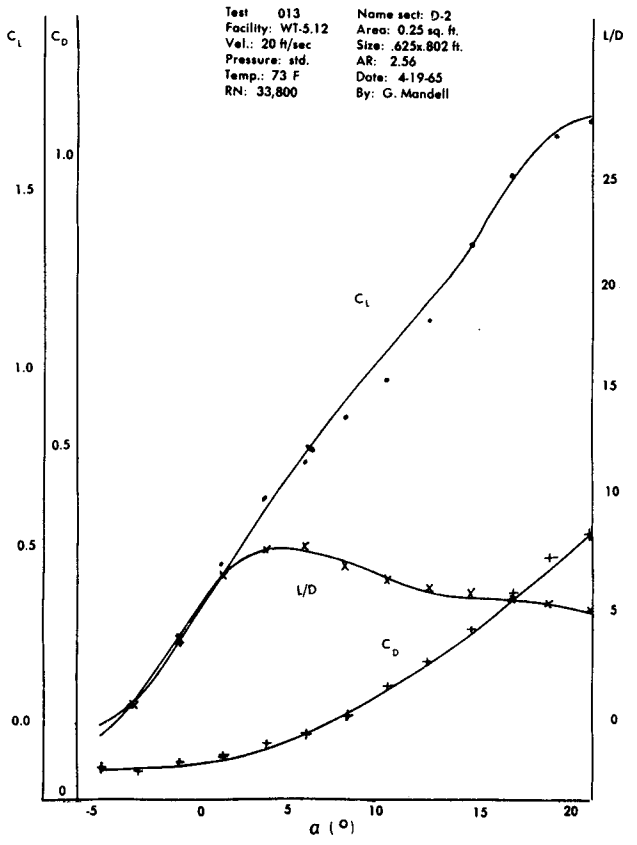
Test 013
Facility: WT-5.12
Vel.: 20 ft/sec
Pressure: std.
Temp.: 73 F
RN: 33,800
Name sect: D-2
Area: 0.25 sq. ft.
Size: .625x.802 ft.
AR: 2.56
Date: 4-19-65
By: G. Mandell
C_L
C_D
L/D
α (°)

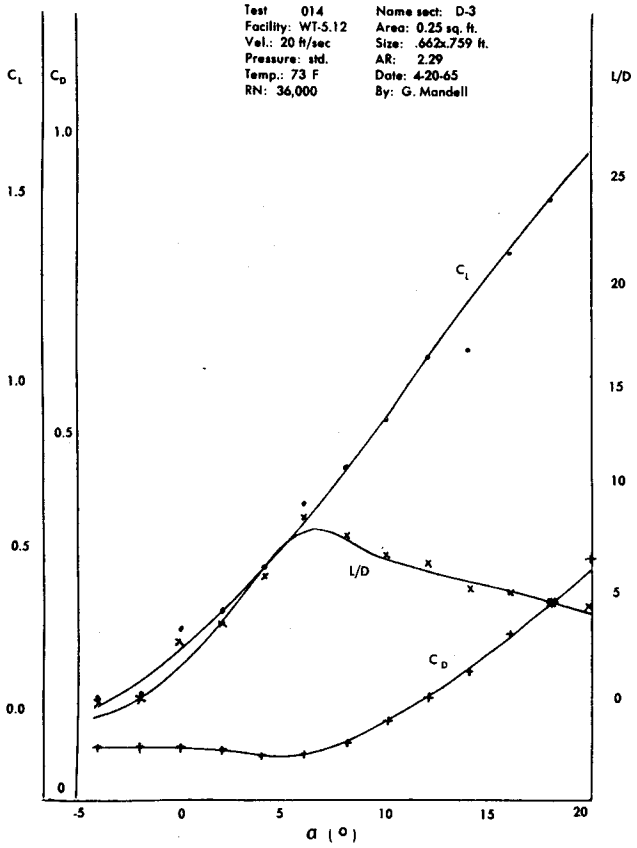
Test 014
Facility: WT-5.12
Vel.: 20 ft/sec
Pressure: std.
Temp.: 73 F
RN: 36,000
Name sect: D-3
Area: 0.25 sq. ft.
Size: .662x.759 ft.
AR: 2.29
Date: 4-20-65
By: G. Mandell
C_L
C_D
L/D
α (°)

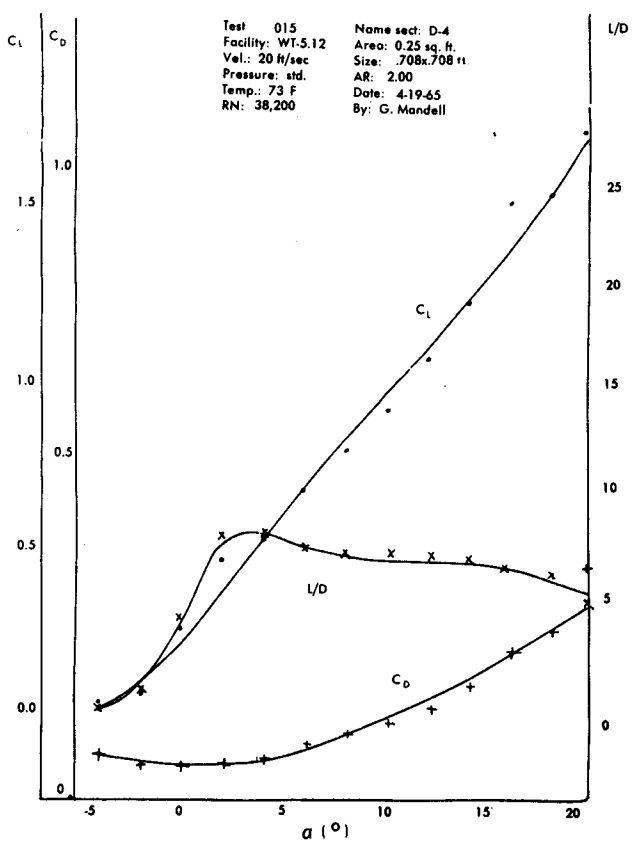
Test 015
Facility: WT-5.12
Vel.: 20 ft/sec
Pressure: std.
Temp.: 73 F
RN: 38,200
Name sect: D-4
Area: 0.25 sq. ft.
Size: .708x.708 ft.
AR: 2.00
Date: 4-19-65
By: G. Mandell
C_L
C_D
L/D
α (°)

Characteristics	Acceptable Range	Optimum Range
VLE	45°-70°	45°-60°
AR	1.37-2.83	2.00-2.83
Wing area	20-40 sq. in.	25-35 sq. in.
Wing loading	0.2-0.6 lb./sq. ft.	0.2-0-4 lb./sq. ft.
Stabilizer area (%WA)	25%-35%	25%-30%
Tail area (%WA)	20%-30%	20%-25%
Elevator area (%SA)	20%-30%	25%-30%
Actuator spring wire diameter	.025"	.025"
Flange width (%cal.)	15%-35%	17%
Flange gap (%cal.)	35%-50%	35%
Fineness ratio	11.0-21.0	11.0-16.0

Interpretive Notes

Flange width: distance sheath plates project from forebody
%cal.: per cent of forebody diameter. One such diameter is defined as "one caliber"
Flange gap: spacing of wing sheath plates off from one another
Fineness ratio: ratio of vehicle length to forebody diameter

Figure 8. Quantitative design criteria for extensible flexwing rocket vehicles.

quite important at these low Reynolds Numbers.

Conclusion; Formulation of Design Criteria

While in general one must be wary of drawing conclusions too sweeping from such limited data, it is certainly true that the investigations to date have made it possible to delineate certain ranges of permissible values for many design features of the extensible flexwing, and to state with reasonable assurance that those vehicles designed within the framework thus established will operate satisfactorily. A synthesis of the flight and laboratory test data has been used to compile in table form such a demarcation of criteria, Figures 7 and 8, appended to this discussion. The tables are, of course, directly applicable only to such small vehicles as used in the author's flight test program; the relevance can however, readily be extended to larger, higher-weight models by due consideration of scaling factors with which every experienced aeromodeler is familiar. This study and its results are, therefore, considered to comprise a significant advance in the state of the art of model rocket recovery by aerodynamic gliding techniques.

Ed. Note: A flexwing boost-glider design article will be featured in an upcoming issue of MODEL ROCKETRY.

Scale Design:

MT-135 Japanese Sounding Rocket

George Flynn

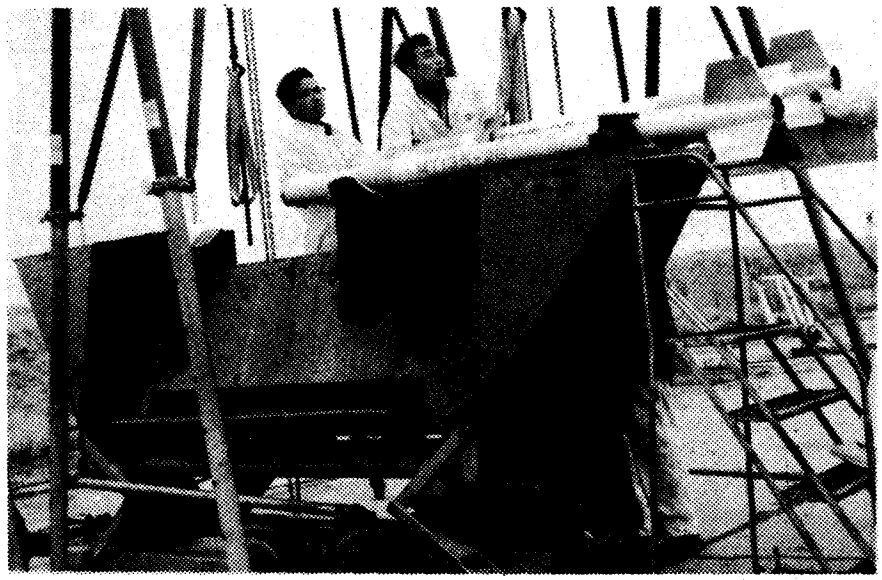

The Japanese MT-135 is a relatively inexpensive, and easy-to-handle, single-stage, sounding rocket. Use of a low burning rate, high specific impulse, solid propellant, as well as an airframe which has low drag, enables this rocket to carry a 3 kg (6.6 pound) payload to about 200,000 feet.

The MT-135 was designed to facilitate wind and temperature measurements in the stratosphere. Generally, the payload consists of an echo-sonde with a resistance thermometer and a 3.5 meter diameter silk parachute. The echo-sonde, operating on 1680 MHz, is a transponder capable of sending analog temperature data. The echo-sonde receives a pulse signal sent from a ground based transmitter and immediately sends back a pulse in order to provide slant range data. After the range pulse, a series of analog data pulses modulated sequentially according to the measured value of temperature is transmitted.

The nose-cone, which is constructed of fiber-reinforced plastic to allow radio transmission through an antenna attached to the echo-sonde itself, is separated from the rocket motor near the peak of the trajectory. Nose cone separation is triggered by means of a pre-set electronic timer, which is started by removing a shorting bar at the moment of launching. All measurements are taken during the descent of the echo-sonde on the parachute.

The pulse signals sent from the payload are received by an automatic tracking parabolic antenna 2 meters in diameter, which provides angular position data on the payload. The slant range is determined by the time delay for the ground pulse to travel from the transmitting antenna to the echo-sonde, where it is received and retransmitted, and back to the ground receiving antenna. The position of the descending echo-sonde is calculated from the measured slant range and angular position. The velocity of the upper atmosphere wind is determined from the motion of the payload as it descends under the parachute.

The first launching of the MT-135 took place from the Kagoshima Space Center, Uchinoura, Japan in July 1964. On this and five successive developmental flights, both the rocket and the meterological payload system were successful. Since then, over 20 MT-135's have carried payloads aloft for the Japanese Meterological Agency.

In 1966 representatives from Japan and the United States met to discuss a cooperative upper atmosphere research project utilizing the MT-135 rocket system and a similar U.S. system (Arcas).

The first two launchings in this joint program took place on March 21, 1967, just 10 days after the Japanese scientists and their rockets arrived at Wallops Station. The purposes of these launchings were:

1) to compare and cross-calibrate data from the Japanese MT-135 system and the U.S. Arcas system,

2) to verify the flight and operating conditions of the rockets,

3) to obtain new information on the operation of each of the meterological rocket systems as a whole, and

4) to obtain additional data on the day-night cycles of wind and temperature in the stratosphere.

Nine more MT-135's, along with a similar number of Arcas rockets, were launched during the 19 hour period from 4:10 am to 10:58 pm EST on April 4, 1967. Six of the MT-135 rockets successfully carried their radiosondes to about 60 km.

The MT-135 is well suited for scale model flying, and will perform well in altitude or payload competitions. This rocket can easily reach over 2000 feet with Flight Systems E or F engines. The only painting information we have is from black and white photographs of the Wallops Station series of MT-135's (see illustrations). In these, the nose cone appears to be silver, with a dark tip. The rocket body and fins are white, and the lettering JAPAN/UNITED STATES 28 is stenciled down the length of the rocket.

References

Spurling, John and Arizumi, Naosuki, The Japan - United States Meterological Rocket Project, paper presented at the Seventh International Symposium on Space Technology and Science, Tokyo, Japan, May 1967.
Tamaki, Namura, and Arizumi, MT-135 Meterological Sounding Rocket, SES Record 0001, The Institute of Space and Aeronautical Science, University of Tokyo, June 1965.
Press release and relate information supplied from the Public Information Office, NASA Wallops Station.

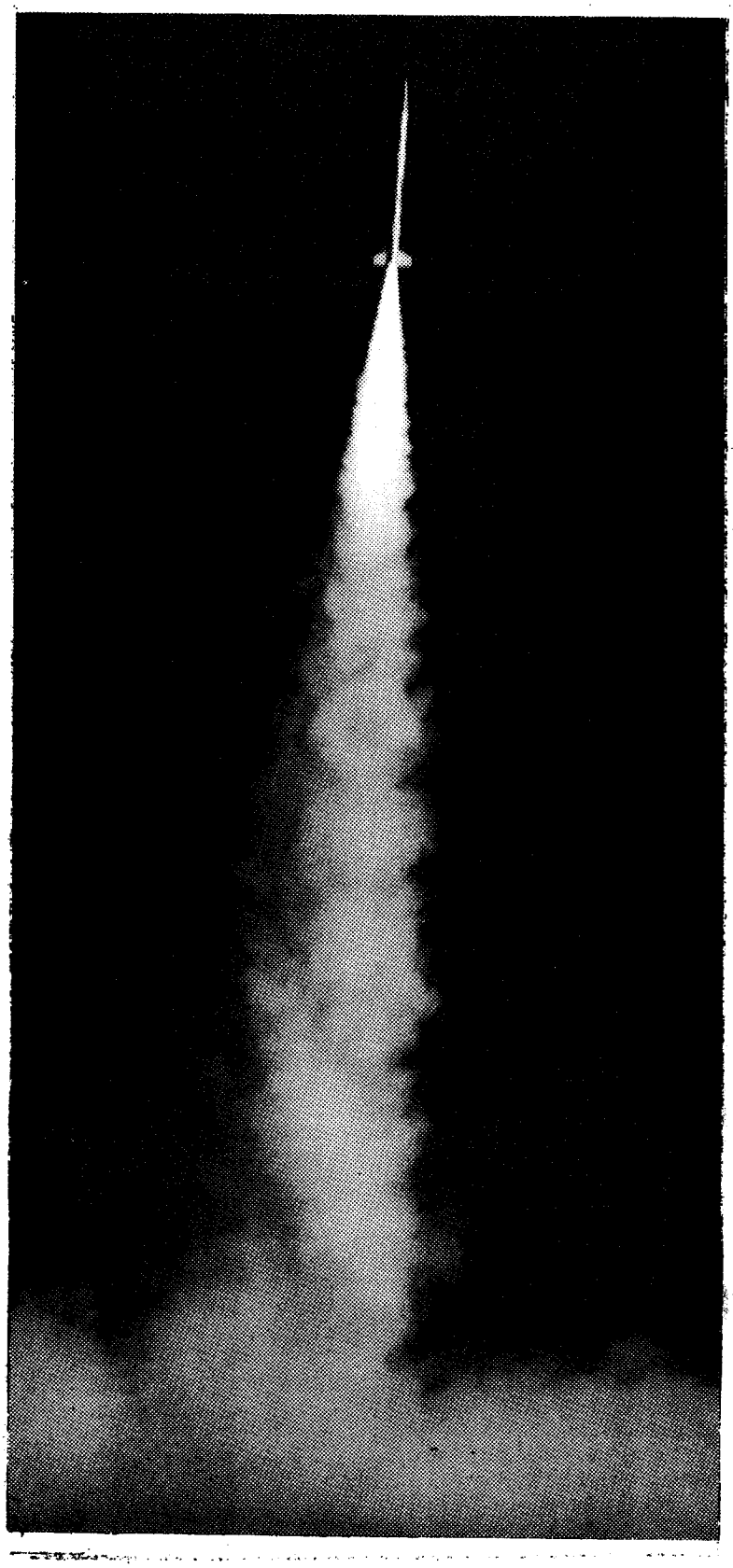

NASA Photos

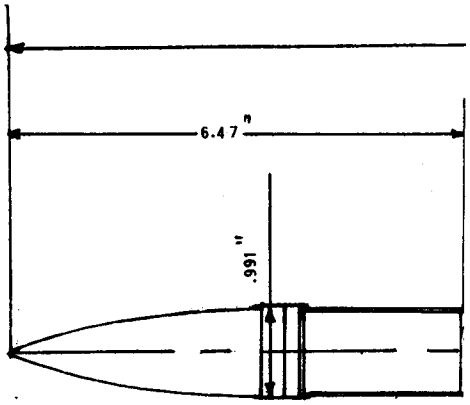

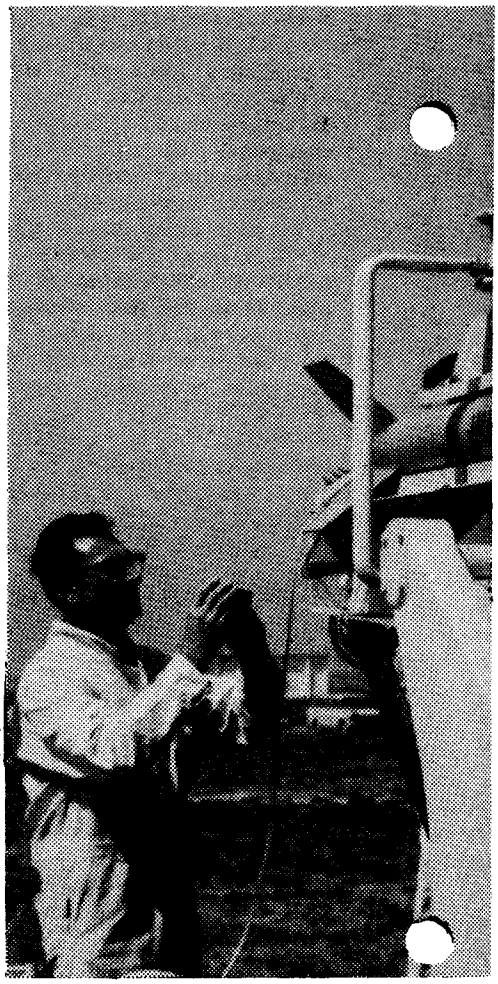

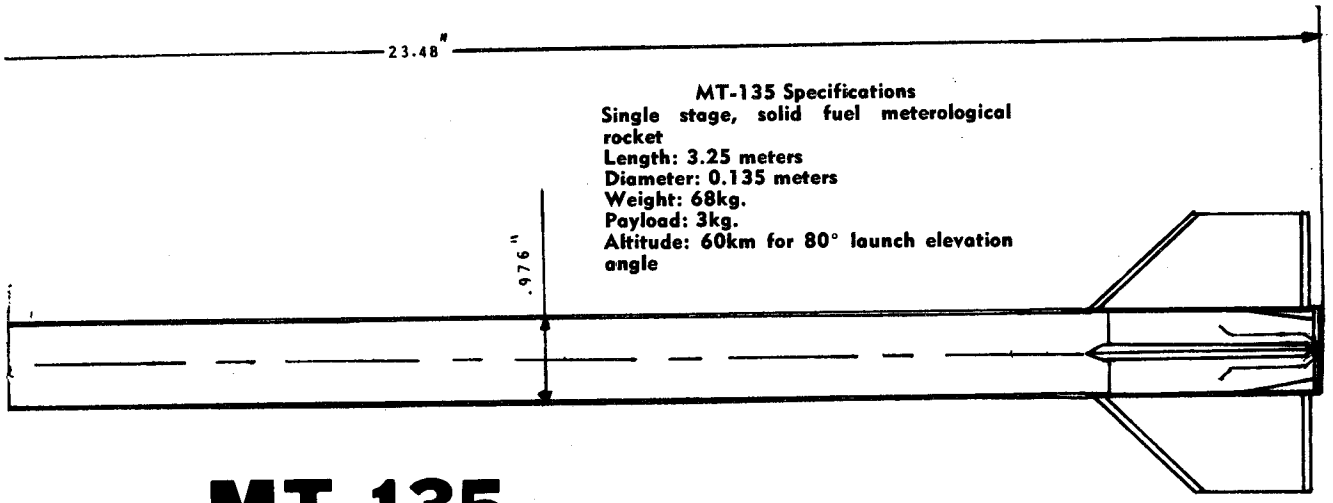

MT-135 Specifications
Single stage, solid fuel meterological rocket
Length: 3.25 meters
Diameter: 0.135 meters
Weight: 68kg.
Payload: 3kg.
Altitude: 60km for 80° launch elevation angle

MT-135

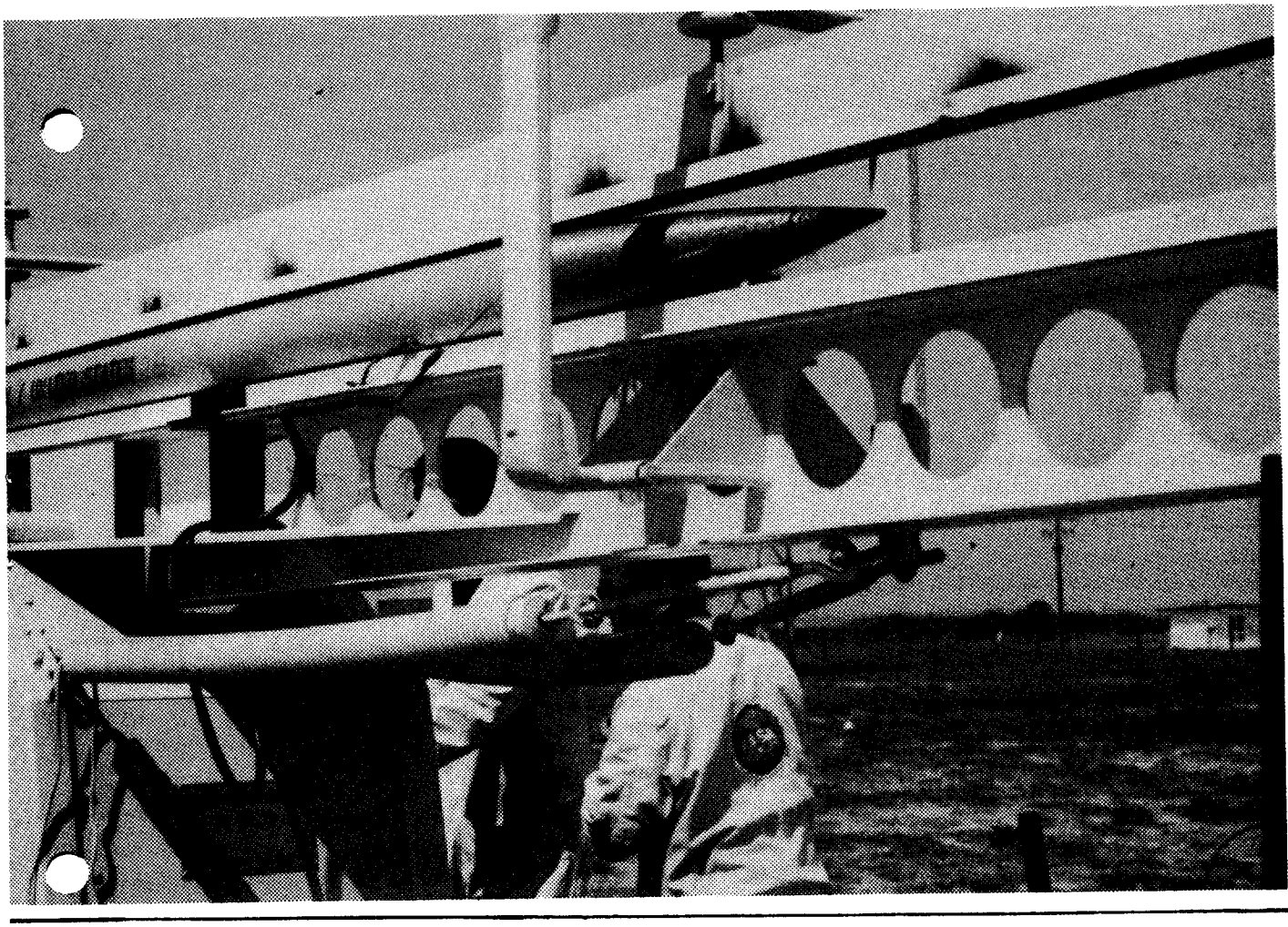

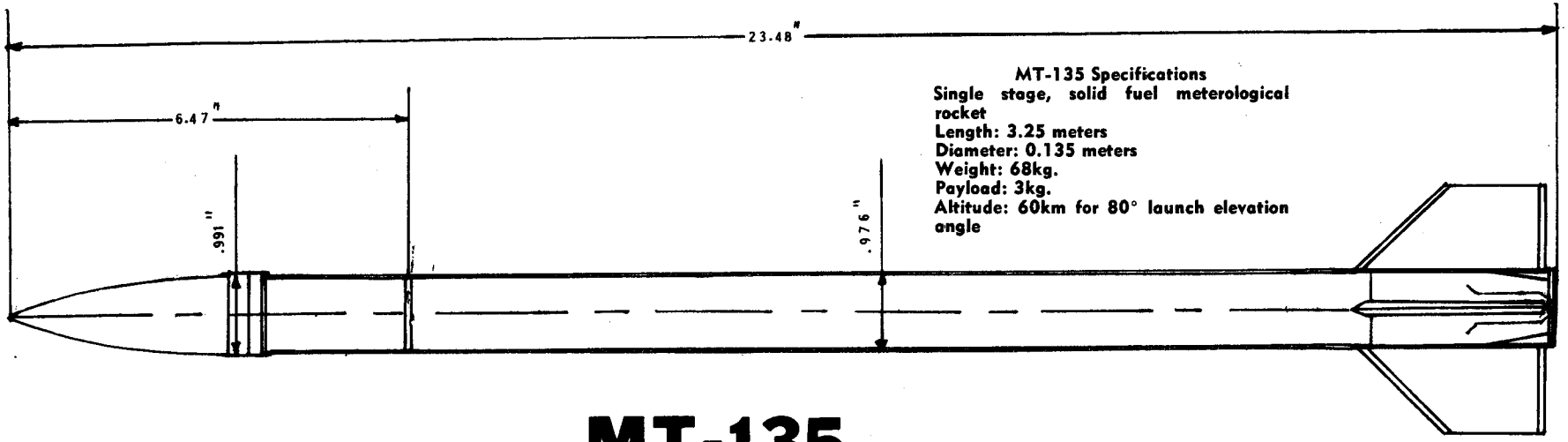

MT-135 Specifications
Single stage, solid fuel meterological rocket
Length: 3.25 meters
Diameter: 0.135 meters
Weight: 68kg.
Payload: 3kg.
Altitude: 60km for 80° launch elevation angle

MT-135

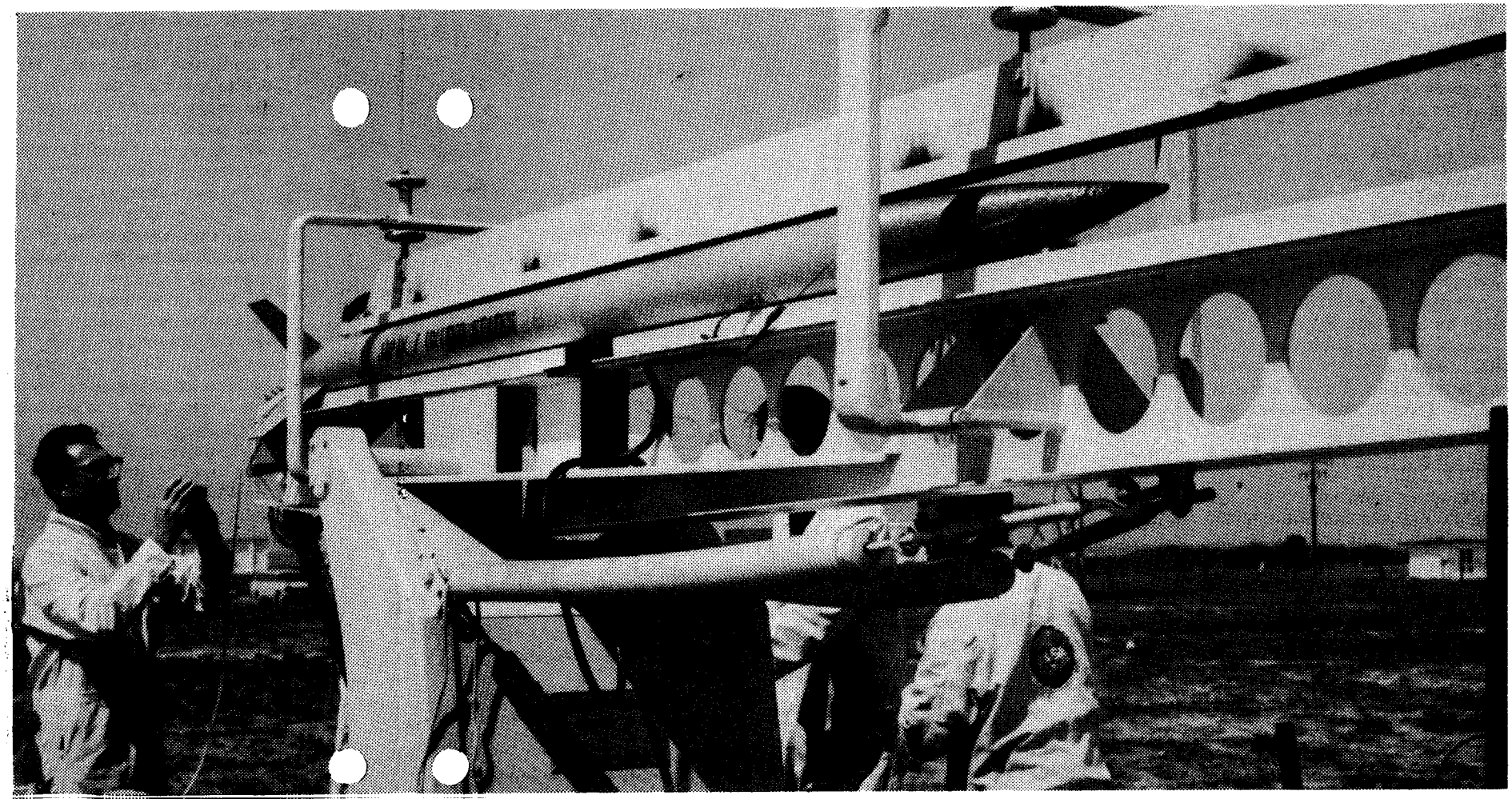

Calculating Drag Coefficients

George Caporaso

At present there are many good closed form solutions that can be used to find the altitude that a model rocket is capable of attaining.[1] Their success depends on the availability of an accurate value of the drag coefficient of the rocket in question.

One method for determining drag coefficients of model rockets has already been published.[2] This article will present an alternate method.

The present technique consists of separating the drag into its various components and finding each component's contribution to the total drag. We may start by listing the various components. They are:

1. shell resistance (pressure drag plus base drag)
2. friction drag of the body
3. friction drag of the fins
4. vortex drag of the fins
5. interference drag of the fins
6. parasite drag (of launch lug, etc.)

The shell resistance is almost totally composed of the base drag, the shape of the nose cone mattering very little as long as it is reasonably long and slender. That is, if the base cross-section area equals the frontal cross-section area, then the shell resistance coefficient is relatively independent of the shape.

So, if the base area Ab is equal to the frontal cross-section area Af, the shell resistance drag coefficient would be given by (1) where K(V) is plotted in the accompanying graph.[3] If Ab is smaller than Af and there is no abrupt change in cross section over the rocket body from Af to Ab, then the shell resistance coefficient is given by (2).[4]

Next, the friction drag of the cylindrical body must be calculated. This drag component does not include the friction drag on the nose cone which is very small and is included in the shell resistance coefficient. The friction drag coefficient for the body is given by (3) where Abd is the total surface area of the body and RN is the Reynolds number which is equal to 532 X V(ft./sec.) X Length (inches).[5] To evaluate this formula, assume an average value of the rocket's velocity to be 350 ft./sec.

Now the drag of the fins must be calculated. The friction drag component of the fins is given by (4) where Afn is the sum total area of all the fins; i.e., the area of both sides of one fin added together multiplied by the number of fins.[6]

Since there is no good analytical method of accounting for the vortex drag, the interference drag, or the parasite drag, we will overestimate this (safely) by multiplying the friction drag term (4) by 2. The total drag coefficient is then given by (5).

(1) $C_{ds} = 4,860K(V)$

(2) $C_{ds} = 4,860K(V) - 0.20(1 - Ab/Af)$

(3) $C_{dbd} = \dfrac{0.455\ (Abd/Af)}{[\log_{10}(RN)]^{2.58}}$

(4) $C_{dfn} = \dfrac{1.327\ (Afn/Af)}{\sqrt{RN}}$

(5) $C_d = C_{ds} + C_{dbd} + C_{dfn}(2)$

1. "The Exterior Ballistics of Rockets" by Davis, Follin and Blitzer, 1958 D. Van Nostrand Co. page 50.
2. Ibid
3. "Exterior Ballistics Tables Based on Numerical Integration" vol. I, Ordnance Department, U. S. Army.
4. "Resistance of Slender Bodies Moving with Supersonic Velocities, with Special Reference to Projectiles" by Theodore von Karman and N. B. Moore, Trans. of ASME Vol. 54, pp. 303-310, 1932.
5. "Aerodynamic Theory" by L. Prandfl and W. F. Durand, vol. 4, page 153, 1935.
6. "Applied Hydro and Aeromechanics" by Prandlt and Tietjens, Dover 1934, p. 94.

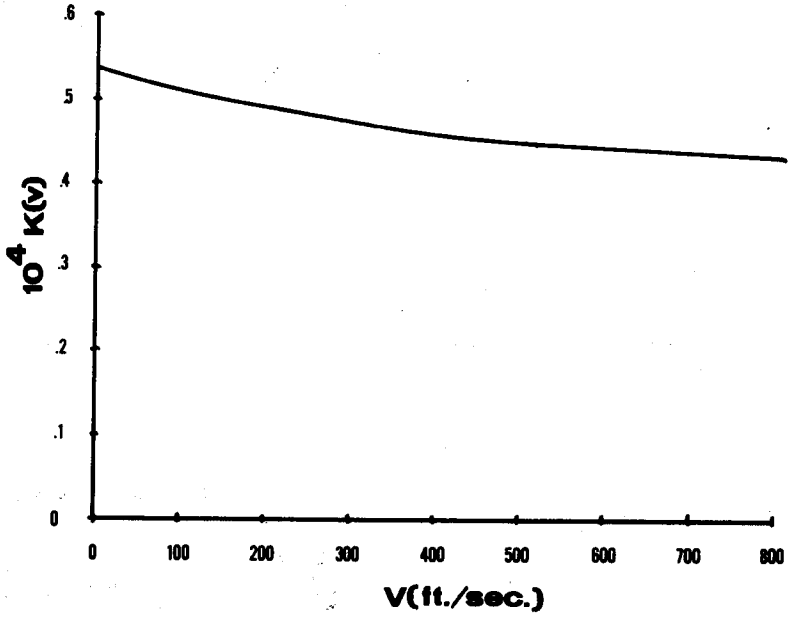

q & a

Having read the first installment of your series on model rocket dynamics, I would like to know how I can determine the dynamic parameters of my models. Could I do this from experiments based on your introduction of the dynamic constants?

A. N. Salina, Kansas

Not in general; the introductory explanations given in the first installment were intended solely to introduce the concepts of the dynamic parameters. Most experiments based on these explanations are either impractical or give erroneous numerical answers. Moments of inertia are usually calculated by mathematical formulae. The corrective moment coefficient can be experimentally determined by measurements based on the explanation of the first installment of the dynamics series. The damping moment coefficient, however, must be determined by an indirect method which will be given in the third installment.

Any questions submitted to this column and accompanied by a self-addressed, stamped envelope will be personally answered. Questions of general interest will also be answered through this column. All questions should be submitted to:

Q and A
MODEL ROCKETRY MAGAZINE
Box 214
Boston, Mass. 02123

Versitex

John Starling

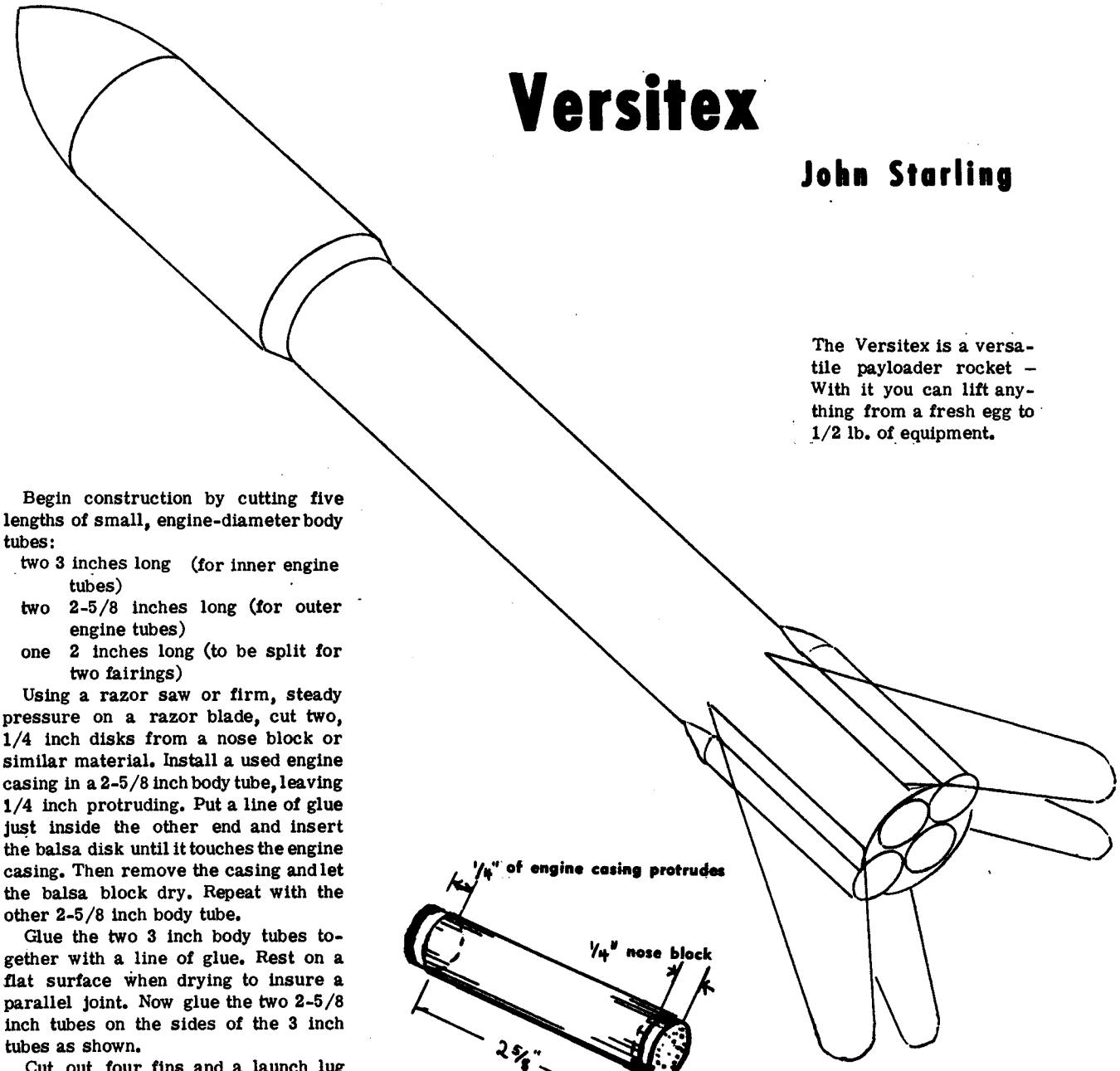

The Versitex is a versatile payloader rocket – With it you can lift anything from a fresh egg to 1/2 lb. of equipment.

Begin construction by cutting five lengths of small, engine-diameter body tubes:

two 3 inches long (for inner engine tubes)
two 2-5/8 inches long (for outer engine tubes)
one 2 inches long (to be split for two fairings)

Using a razor saw or firm, steady pressure on a razor blade, cut two, 1/4 inch disks from a nose block or similar material. Install a used engine casing in a 2-5/8 inch body tube, leaving 1/4 inch protruding. Put a line of glue just inside the other end and insert the balsa disk until it touches the engine casing. Then remove the casing and let the balsa block dry. Repeat with the other 2-5/8 inch body tube.

Glue the two 3 inch body tubes together with a line of glue. Rest on a flat surface when drying to insure a parallel joint. Now glue the two 2-5/8 inch tubes on the sides of the 3 inch tubes as shown.

Cut out four fins and a launch lug standoff from 1/8 inch balsa sheets, as shown in the full size patterns. (The best way to copy the pattern is to cut it out and draw a line around the pattern on the balsa sheet.)

Shave and sand the edges of the fins to an airfoil shape. Leave at least 1/32 inch thickness at the trailing edge to prevent nicks. Round the leading edge to an elliptical cross section.

Use approximately 18 inches of cluster size body tube for the rocket body. (Estes BT-60, Centuri ST 1618, RDC G-16, etc.) Scribe 9 marks on one end as shown on the marking guide: 4 marks for cutting the tube, 4 marks for fin placement, and a mark for the launch lug position.

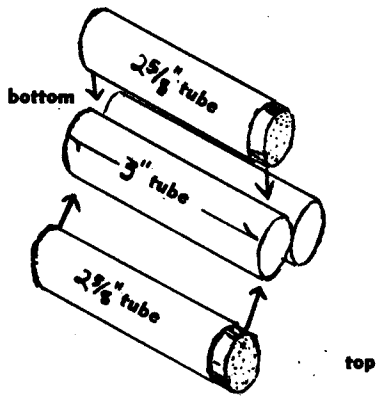

Versitex Parts List

18 inches Cluster size body tube (1.6 inch diameter)
app. 18 inches Engine size body tube (.7 inch diameter)
Payload section to fit body tube
2 18 inch plastic parachutes
nose block for outer engines
lengths of shock cord
engine holders
fin stock
snap swivels
launch lugs
cardboard
adhesive tape

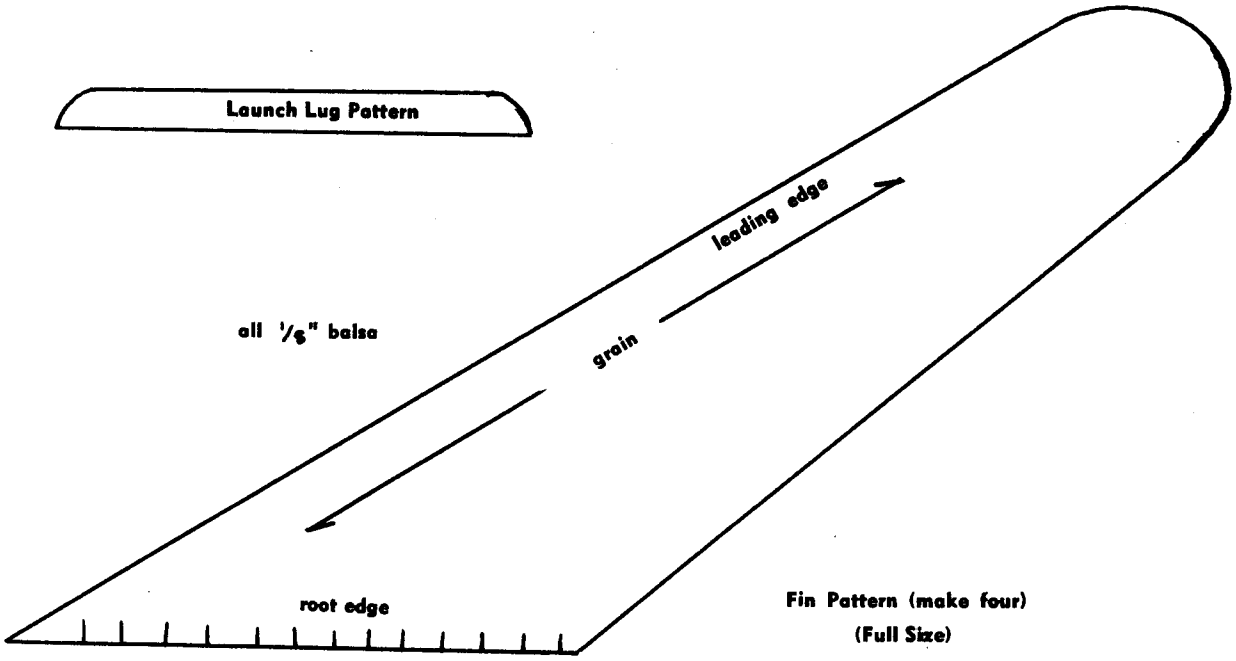

Fin Pattern (make four)
(Full Size)

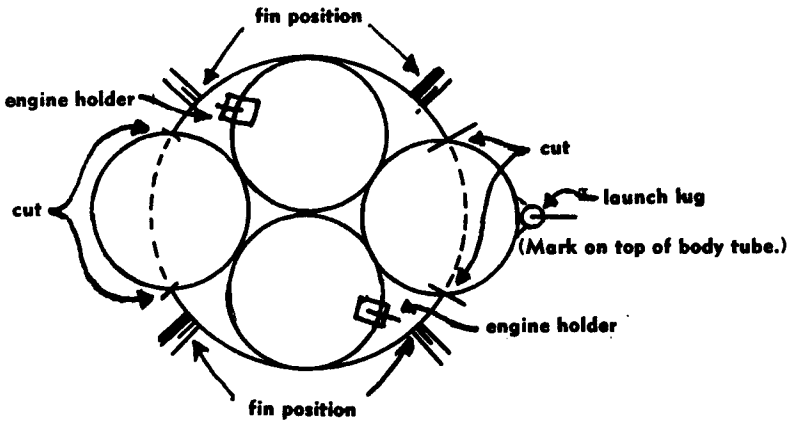

Body Tube Marking Guide

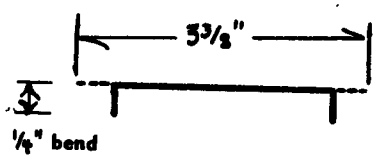

engine holders (2 required)

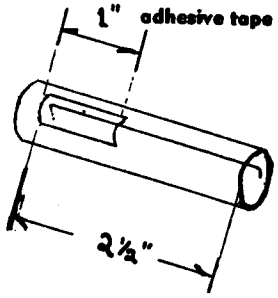

Engine Holder Positioning

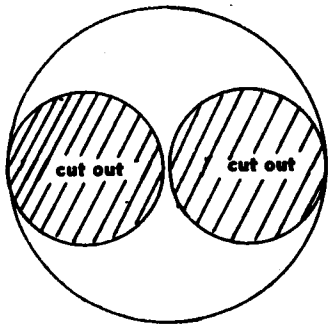

Gas Seal Pattern

Next, draw 3-inch lines at each "cut" mark, using the corner of a drawer or the edge of a board to keep the lines parallel to the body tube. Draw 4 inch lines at each "fin" mark. Then make a mark 3 inches down from the opposite end of the body tube. (This will be where the forward launch lug goes.) Now draw a line around the body tube, 2-3/4 inches up from the tube bottom. The two areas show in the diagrams are to be removed. Cut them carefully and sand any rough edges.

Construct two engine holders by cutting 2 pieces of music wire 3-3/8 inches long. Bend 1/4 inch of each end at 90 degrees. (Engine holders are also available ready for installation from Estes Industries: Cat. #651-EH-2.)

Mark the top of the engine holder assembly (the end with the balsa blocks) for placement of the engine holders. Place them where there is enough freedom to move them when installing engines.

Install the engine holders on the inner body tubes by making 1/4 inch slits in these body tubes 2-1/2 inches from the bottom. Install one end of a holder in each slit and tape down that end with 1 inch of adhesive tape. The other 1-1/2 inches must be free to allow the holder to flex to permit removal of engine. When positioning is judged correct, glue down the edges of the tape with white glue.

Next, copy the gas seal pattern onto stiff cardboard and cut it out with a sharp knife. Slip this over the front end of the engine tube assembly and glue in place. This seals off the ejection gases.

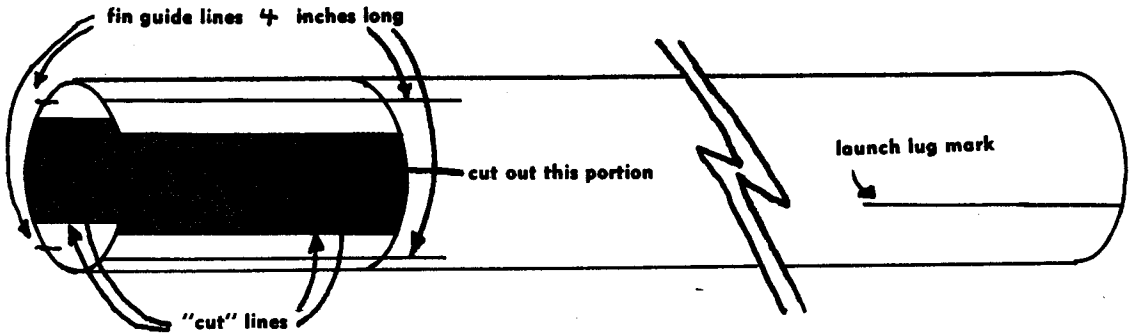

Test fit the engine tube assembly into the rear of the body tube so that it is a flush fit. If necessary, sand edges of the gas seal or deepen the slots in the large body tube.

Apply glue to the edge of the gas seal and insert the assembly. Be certain that the assembly is centered. Apply glue along the 4 cuts in the large body tube.

Attach fins in the usual manner. Apply a thin line of glue along the root edge and hold it against the body tube for about 30 seconds. Make sure that it is straight and on the line. Repeat for the other 3 fins. Balance the rocket upside down and make certain that the fins stay perpendicular to the body tube as the glue sets.

Split the remaining 2-inch piece of small diameter body tube lengthwise. Trace around the fairing pattern onto the inside of each half. Then cut out with a knife. Trim for a good fit aginst the body tube. The balsa disks may be bevelled for a better fit. Glue the two fairings in place.

Cut a piece of launch lug 2-5/8 inches long and another 2 inches long. The front end of the 2-5/8 inch piece may be trimmed at an angle. Glue the 2 inch piece to the launch lug standoff made from 1/8 inch balsa. Glue this on the line at the front of the rocket body tube. Glue the other launch lug to the side engine tube. The two launch lugs must be in line.

Now attach the static line (24 inches of thick thread or other strong line). Thread the line through a large needle. Push the needle back and forth through a fin. Start 1 inch from the leading edge of the fin and as close to the root edge as possible. Tie as shown. Carefully pull tight so as not to tear the balsa.

Apply fillets to the fins. Support the rocket on its side while the fillets dry.

Assemble the payload section from a commercially made unit, as shown in the diagram. Two recovery systems are used with the Versitex, one for the payload and one for the rocket. A shock cord is attached to a screw eye in the rear of the payload compartment, and an 18 inch chute is attached with a swivel to the shock cord. The other end of the shock cord is tied to the static line sewn into the fin.

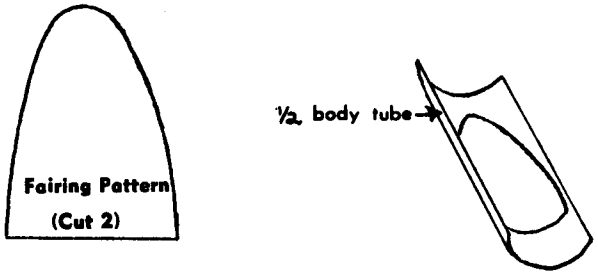

Cut fairing pattern out of ½ body tube (2")

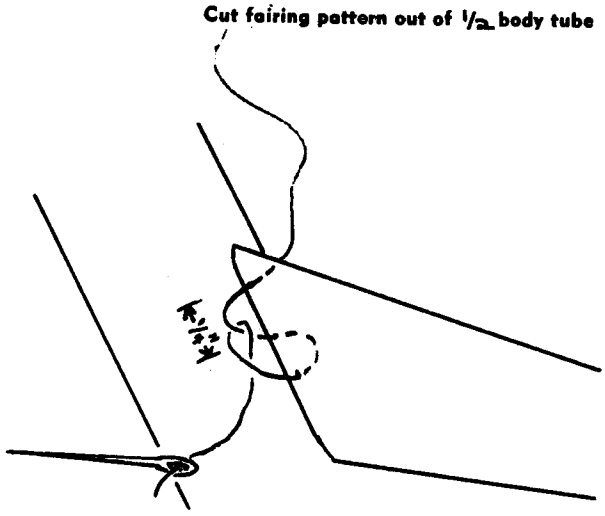

Static Line Attachment to Fin

Now apply more glue to all fin-body joints, launch lugs, and along all edges of the fairings and slots.

Finish the Versitex in the usual manner. Apply balsa fillercoat to all exposed balsa. Sand and repeat until grain is filled. Give the rocket a light coat of dope, lacquer, or enamel in desired color. Additional coats may be applied for color depth. Use a rubbing compound and wax if desired.

This rocket may be flown with either 2 or 4 engines. The side engines are expelled at ejection or at burnout (When used as side boosters). For high accellerations studies, use 4 B 14-5's (old classification B 3-5). For high altitude payload flights, use B 14-0's in the side tubes and B 4-2's, B 4-4's, C 6-5's, or C 6-7's in the center tubes. Choose the delay time according to payload weight. The Versitex has been successfully flown with a 1/2 lb payload, to study heavy weight affects. The Versitex, however, is gentle enough to loft an egg.

To launch the Versitex, hook up igniters as you would for any cluster-engined rocket. Use a launch stand that will be stable enough to launch this big rocket, especially if you are using a heavy payload. –

NFPA Adopts Model Rocket Code

Unfortunately, despite the perfect safety record of model rocketeers since the development of model rocketry, many states still have laws on the books making all rocketry illegal. Nearly all of these laws were originally passed to outlaw dangerous homemade propellants, as suggested by the National Fire Protection Association. The NFPA now recognizes and supports safe model rocketry and again presents to the states a suggested code for the regulation of rocketry. This new code, legalizing model rocketry, is a milestone in expanding our hobby-science.

The new official "Code for Model Rocketry," containing measures to safeguard this popular and growing activity, has just been published by the National Fire Protection Association (NFPA).

Adopted at the 1968 NFPA annual meeting, the code has the two-fold purpose of prohibiting the making and launching of dangerous homemade "rocket bombs" and of eliminating the deaths and tragic injuries to young people that have occurred because of experiments with explosive "rocket fuels," home manufacture of rocket engines, and attempted launchings of these homemade devices.

Recognizing the constructive value of safely-conducted model rocket activities, the 20-page text of the new code applies to model rocket engines, to rockets propelled by these engines, and to launching and testing operations.

There are standards covering design, construction, limitation of charge and power, and reliability of all model rocket engines manufactured for sale, as well as guidelines for design and construction of model rockets using these engines. The new code also includes material on the conduct of launchings, tests and other operations so that hazards are minimized.

As emphasized in the foreward to NFPA "Code for Model Rocketry," "These safer model rocket activities should not be confused with the hazardous, uncontrolled operations of so-called 'basement bombers' and 'amateur rocketeers' who attempt to make their own rocket propellants, motors, and large metallic rocket vehicles."

This code is expected to be widely adopted as the basis of state regulations governing model rocketry, "to safely guide our science-minded youth and citizens." The code is the work of the NFPA Committee on Pyrotechnics, headed by Major Carroll E. Shaw of the Connecticut State Fire Marshal's Office, Hartford.

Copies of the 1968 edition of the new "Code for Model Rocketry (NFPA No. 41 L)" (20 pages, 50 cents) are available from the National Fire Protection Association, 60 Batterymarch Street, Boston, Mass. 02110

SOLICITATION OF MATERIAL

In order to broaden and diversify its coverage of the hobby, MODEL ROCKETRY is soliciting written material from the qualified modeling public. Articles of a technical nature, research reports, construction and scale projects, and material relating to full-scale spaceflight will be considered for publication under the following terms:

1. Authors will be paid for material accepted for publication at the rate of forty cents (40c) per column inch, based on a column of eight-point type thirteen picas wide, for text and one dollar fifty cents ($1.50) per line cut for drawings accompanying text. Payment will be made at the time of publication.

2. Material submitted must be typewritten, double-spaced, on 8.5 x 11 inch paper with reasonable margins. Drawings must be done in India ink and must be neat and legible. We cannot assume responsibility for material lost or damaged in processing; however our staff will exercise care in the handling of all submitted material. An author may have his manuscript returned after use by including a stamped, self-addressed envelope with his material.

3. Our staff reserves the right to edit material in order to improve grammar and composition. Payment for material will be based upon the edited copy as its appears in print. Authors will be given full credit for published material. MODEL ROCKETRY will hold copyright on all material accepted for publication.

Model Rocketry Magazine
P.O. Box 214
Boston, Mass., 02123

High Quality Aerial Photography

Richard Q. Fox

Aerial photography and model rocketry were combined on a practical basis when Estes Industries developed the Camroc in 1964. Since that time, thousands of inspired model rocketeers have attempted to take aerial pictures of their backyards, high school parking lots, and local abandoned fields. Many of these potential reconnaissance flyers, however, were very disappointed with their results, and their Camrocs now sit abandoned along side their slot cars. The reasons for their disillusionment are varied, but all of their difficulties can be overcome.

The Camroc

As a starting point in developing a high quality aerial photography device the suitability of the Camroc should be considered. The Camroc is one of the cheapest cameras on the market. It is designed for use with model rockets, it is light weight, and it has a shutter which is fast enough to prevent motion blurring of its photographs. However, the Camroc breaks readily when dropped from an altitude of 600 feet onto hard pavement, it takes special film which needs processing half-way across the continent, and it cannot be pointed at a specific target with predictable accuracy.

The Camroc's ready-made shutter, film loading system, light weight, and rocket-oriented design make it desirable to use for aerial photography, provided its faults are overcome.[1]

THEORY

The first step to obtaining good photographs is to understand the operation of the Camroc. The Camroc takes a single black and white photograph at the moment of parachute ejection of the rocket. As the photograph is taken, light passes through the clear plastic nose window, through the shutter, through the iris (lens opening), through the plastic lens, and onto the film. The film reacts chemically with the light. In order to obtain a good picture, the proper amount of light must reach the negative. In addition, this light must be in focus, and must not move across the negative as it is admitted.

The parameters of the Camroc are: a focal length of 76 m.m., a shutter speed of 1/1600th of a second (this is three to five times faster than most box cameras), and a lens opening of f-16. These parameters are very well suited for the type of work that the Camroc is designed to do. The fast shutter speed is necessary to prevent motion blurring, and the small lens opening is necessary because of the type of shutter used. I have found that if the lens opening is enlarged a small amount (by drilling), the photographs look as though they are motion-blurred. This is because enlarging the lens opening of a focal plane shutter system increases the effective time that the shutter is open. In other words, the fast shutter acts as if it were too slow.

The Best Lighting Conditions

The key factor to good Camroc photographs is how much light is admitted to the film when the picture is taken. The combination of an f-16 lens opening and a 1/1600th of a second shutter speed does not let in very much light. In fact, if Verichrome Pan film is used in the Camroc, the film will record no image at all! On a typical sunny day, a film with an ASA speed of 1200 is necessary to develop a high contrast photograph. When Estes processes their film, they use a film capable of being processed to ASA 1200. However, if a Camroc photograph is taken on a cloudy day or within two hours of sunset or sunrise, a very disappointing photograph of barely distinguishable objects will be the result. The above problem is perhaps the biggest cause of poor Camroc photographs. Camroc aerial photographs must be taken in bright sunlight during the middle of the day.

Developing the Film

Most amateur photographers are very anxious to develop their own Camroc photos. Much faster results, more control over the end product, and less expense are a few of the advantages of developing your own film. Estes suggests developing their film in Kodak HC-110 developer; however, I have had much better results using Acufine developer. Acufine is a film developer which multiplies the effective ASA of the film being developed. Estes' "Astropan 400" film is identical in speed to Kodak Tri-X sheet film; Tri-X has an ASA rating of 400, but when developed in Acufine developer, it has an ASA rating of 1200. ASA 1200 is exactly the film speed necessary to produce sharp pictures on a sunny day with the Camroc.

The darkroom procedure for Acufine developer and Tri-X film is to develop the film in a tank for six to nine minutes, agitating for five seconds every minute. The precise developing time depends, among other things, on the strength of the rubber band in the shutter of the Camroc being used, the age of the developing solution, and the brightness of the subject of the picture. Try a nine minute developing time, and cut the time back if nine minutes produces too dense a negative. Washing and fixing the negative is done in the standard manner described on the

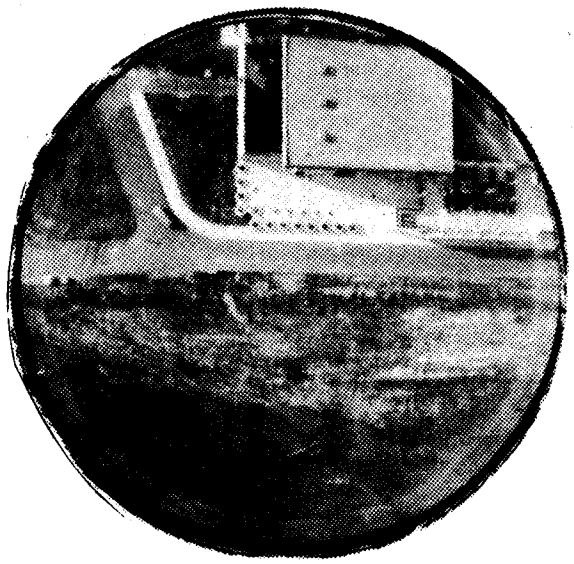

Photo taken with a modified Camroc

1.) Modifying a cheap box camera for rocket flight is very difficult, and very clumsy. The result is a heavy payload and motion-blurred pictures.

Tri-X film instruction sheet. This film developing procedure has produced the best negatives I have seen.

Cutting Film Disks

Amateur photographers may wish to go one step further, and cut their own film disks. This is accomplished most easily by machining a disk cutting tool on a lathe. This tool consists of a three to five inch long bar of steel which has a 1-3/4 inch or larger radius. The end of the bar is machined flat except for a sharp 1-1/2 inch diameter ridge centered on the end of the bar. When the end of the bar is hammered against the Tri-X film sheet or roll, a disk of film will be cut out. Of course, the cutting procedure must be carried out in the dark. The cutting tool works best when the film to be cut is placed on a slab of linoleum which in turn is placed on the darkroom floor. The floor supports the film against the hammer blow and it absorbs less of the shock of the blow than a table would. The linoleum provides a good surface for the cutting edge to continue into after it has cut through the film.

A Better Lens

The lens that Estes supplies with the Camroc is molded out of clear plastic. Its quality varies from one Camroc to the next. The pictures taken through Estes lenses frequently do not have sufficient sharpness to enlarge beyond a factor of two. For this reason it is desirable to substitute a high quality glass lens in the Camroc.

Glass lenses are available from several sources, including Edmund Scientific Co. of Barrington, N. J. The most desirable glass lens would be an achromatic glass lens with a focal length of 72 mm., and a diameter of between 10 and 30 mm. A second source of lenses is old cameras. Several models of plastic box cameras have lenses that fit the bill perfectly. One disadvantage of using glass lenses is that Estes film can not be used with them in the Camroc. The Estes film disk bends into a concave shape when placed in the film holder. This is desirable because the Estes plastic lens has a concave focal plane. Glass lenses have a flat focal plane and therefore flat film disks should be used. Flat film disks are obtained by cutting Tri-X film to a diameter which is slightly smaller than that of Estes film. The diameter of the film disks should be such that they do not bend out of their plane when placed in the film holder.

Making an adapter to hold a glass lens in a Camroc is a tricky problem. Machining an adapter out of plastic stock is the most accurate and sturdy method. However, for this or any other method, the lens must be positioned at a distance that is precisely the focal distance away from the film. To do this, machine the lens holder so that it holds the lens a little too close to the film. Then take a picture, on the ground, inspect the developed print for the degree of sharpness, and machine the lens mount so that the lens is a few thousandths further away from the film. Take a picture with the lens in its new position, and again inspect the picture for the degree of sharpness. By repeating this procedure three or four times, a lens setting that produces very sharply focused pictures can be arrived at. This procedure takes several hours to carry out, but the results are well worth it.

Launch Vehicles

Putting the best camera in the world on top of a model rocket will not do any good if the camera takes a picture of the sky, or a picture of the crater it has dug in the ground. Choosing a vehicle, and engines with the proper time delay, is an important part of obtaining good aerial photographs. For single stage flights, the best engines are the Estes or Centuri C6-7 and the Flight Systems D1.12-6 (English units). For two stage flights, combine the B14-0 and the C6-7 or the Flight Systems D1.12-0 staged with a C1.75-6 or the D1.12-0 staged with a D1.12-8. This last combination will predictably take the Camroc to an altitude of 1800 feet.

When designing the vehicle, be sure not to make the fins larger than necessary for a stable flight. Large fins tend to cause weathercocking and also to send the rocket into an overdamped oscillation.

Infra-Red and Color Film

A good area for research would be in the use of infra-red and color film with the Camroc. Infra-red film is especially desirable because in the infra-red spectrum, vegetation and warm objects emit a great amount of light, while cold objects emit very little light. An infra-red aerial photograph of a field can prove to be very interesting. At present, Kodak produces an infra-red film with an ASA rating of 80. It might be possible to obtain a good picture if the film is developed in Diafine developer, which would increase its speed to about 640. The picture would have to be taken on a very hot, bright day, in order to fully expose the film.

Color photography with the Camroc is next to impractical at the moment. The fastest color film which is commercially available has an ASA rating of 500. Any attempts to increase the speed of the film will result in a loss of fidelity of the color. In other words, the picture will be colored, but it will not be an exact color reproduction of the image photographed. One way around the problem is to decrease the shutter speed or to increase the lens opening of the Camroc. Unfortunately, both of these modifications will lead to a blurred picture. An additional drawback to color aerial photography is the comparatively high cost of developing color film.

Color movies have been successfully taken from a model rocket. Several groups are currently working on this project, and model rockets with movie cameras may become common in a few years.

The Camroc modifications which I have outlined here have been carefully tested and developed. Some of the modifications take several hours to correctly prepare, but in the end the results are well worth the effort. The modified Camroc becomes a dependable working tool for further experimentation in the fields of photography, aerial mapping, and even news reporting.

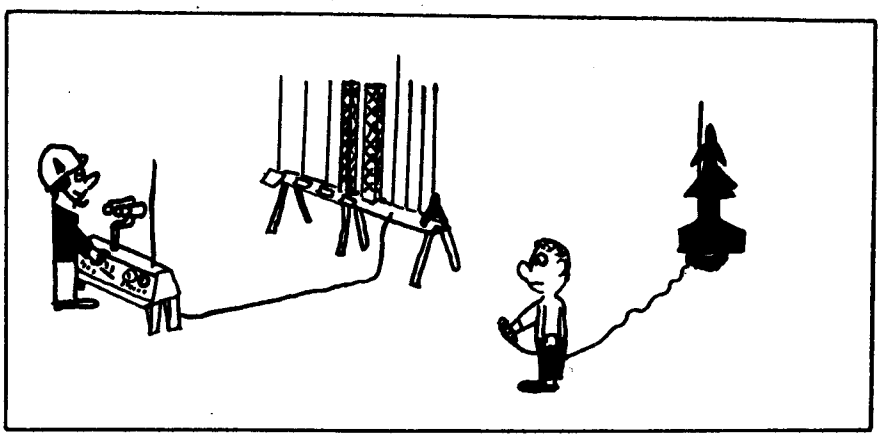

Fundamentals of Dynamic Stability

Gordon K. Mandell

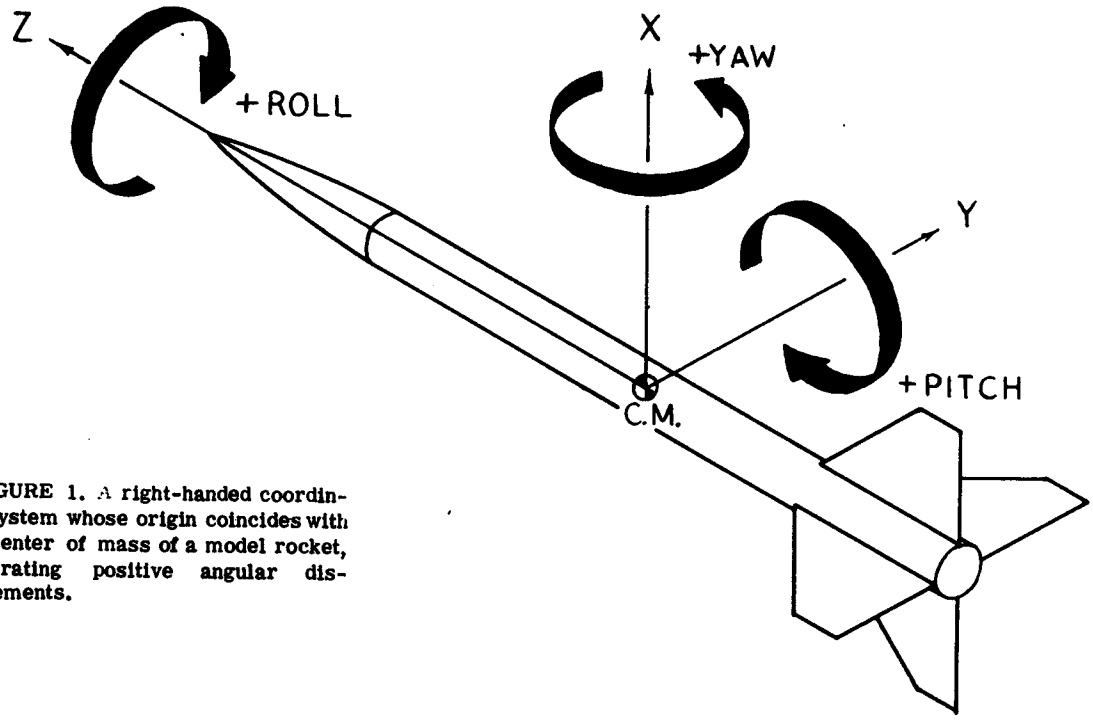

FIGURE 1. A right-handed coordinate system whose origin coincides with the center of mass of a model rocket, illustrating positive angular displacements.

The following article comprises the second section of a three-part treatment of the dynamic behavior of model rockets. Last month's issue carried Part I, in which the dynamic parameters of streamlined projectiles were introduced and the dynamic behavior of models not spinning about their longitudinal axes was discussed. The present treatment will concern itself with the dynamics of rockets having nonzero roll rates, and the third article of the series will discuss the practical interpretation of the mathematical results obtained with reference to designing model rockets for dynamically favorable behavior. The analytical procedures and technical terminology introduced in the course of the first article will be freely used in what follows; it is therefore recommended that the reader become familiar with the first article before attempting the second.

PART II
PROBLEMS IN NONZERO ROLL RATE

Inertial Coupling

The dynamic behavior of model rockets which are spun about their longitudinal axes is fundamentally different from that of those which are not. This is true because a phenomenon known as inertial coupling links pitching motions to yawing motions in such a way that the one cannot occur without the other in a free-flying rocket whose roll rate is nonzero.

To illustrate the effect of coupling we make reference to Figure 1, in which a hypothetical rocket is shown with respect to a coordinate system whose origin coincides with the rocket's center of mass. Suppose this rocket to be held in a system of gimbals such that it is free to yaw and roll, but is restrained from pitching. Suppose, further, that the entire arrangement is suspended in a vacuum so that no aerodynamic forces exist. Now imagine that the rocket has been set to yawing at an angular velocity Ω_X rad/sec by some effect which has since been removed, but that the roll rate has been

kept zero. Under these conditions the rocket will simply continue to rotate in yaw at the rate Ω_X without producing any further effect on the system. No yawing moment will be required to maintain the yaw rate, no rolling moment need be applied to keep the rocket from rolling, and no pitching moment is needed to keep the pitch angle zero. We say, therefore, that no inertial coupling exists.

But suppose the rocket is given a roll rate of ω_Z rad/sec as well as the yaw rate Ω_X – what will happen now? In this case we will find that a pitching moment M_Y given by

$$M_Y = -I_R \Omega_X \omega_Z$$

must be applied to the gimbal system to maintain a zero pitch angle and zero pitch rate. The new system now exhibits inertial coupling.

Consider a similar gimbaling arrangement which permits the rocket to pitch and roll but restrains it from yawing. We again find that, if the rocket pitches at a constant angular velocity Ω_Y without rolling, no moments need be applied anywhere to maintain the state of the system. If a constant roll rate also exists, however, a yawing moment M_X given by

$$M_X = I_R \Omega_Y \omega_Z$$

is required to maintain the apparatus at a zero yaw angle. Again, we have inertial coupling.

In one final experiment we remove the gimbals entirely and, while the rocket is spinning about its longitudinal axis at the rate ω_Z, impart to it either a pitching or yawing angular velocity. Now that the rocket is free there is nothing to keep the pitching motion from affecting the yawing motion and vice versa. The net effect results in a "coning" movement of the longitudinal axis familiar to anyone who has ever operated a toy gyroscope. This motion, called a precession, is obviously quite different from the simple "pinwheeling" maneuver that would result in the absence of roll. As we shall see, the presence of roll also markedly modifies the nature of the movements executed by free-flying model rockets in the atmosphere in response to various disturbances. In the case of a rolling rocket the radial moment of inertia I_R and the roll rate ω_Z join with the dynamic parameters C_1 (corrective moment coefficient), C_2 (damping moment coefficient), and I_L (longitudinal moment of inertia) in determining the character of a model's dynamics*.

Problem 1. Homogeneous Response to General Initial Conditions

The homogeneous, or characteristic, response is the motion described by a model rocket subsequent to its encountering a disturbance in flight which leaves it with some arbitrary initial values of angular displacement and angular velocity in pitch and yaw at a time we shall call zero, although in fact it may be any time during the flight.

The behavior of a spinning rocket in such a case is given by

$$\alpha_X = A_1 e^{-D_1 t} \sin(\omega_1 t + \varphi_1) + A_2 e^{-D_2 t} \sin(\omega_2 t + \varphi_2) \quad (1a)$$

$$\alpha_Y = A_1 e^{-D_1 t} \cos(\omega_1 t + \varphi_1) + A_2 e^{-D_2 t} \cos(\omega_2 t + \varphi_2) \quad (1b)$$

where α_X and α_Y are the yawing and pitching angles in radians, respectively. A_1 and A_2 are called the initial amplitudes of the first and second modes; D_1 and D_2 are the damping coefficients, or inverse time constants, of the first and second modes, ω_1 and ω_2 are the angular frequencies of the first and second modes, and and φ_2 are the phase angles, or "phases," also identified with the first and second modes, respectively. It will be recalled from Part I that e is the base of the natural logarithmic system, numerically equal to approximately 2.718, and that t represents the time elapsed since the initiation of the motion, in seconds.

The angular frequencies and damping coefficients are determined by the values of the dynamic parameters. Because the expressions for the angular frequencies are rather complicated, we shall want to simplify their appearance by the use of an "intermediate" function of the dynamic parameters. This function, which we shall name $\mathcal{F}$, is given by

$$\mathcal{F} = \frac{I_R^2 \omega_Z^2}{4 I_L^2} + \frac{C_1}{I_L} - \frac{C_2^2}{4 I_L^2} \quad (2)$$

The angular frequencies may then be written as

$$\omega_1 = -\frac{I_R \omega_Z}{2 I_L} + \sqrt{\frac{\mathcal{F}}{2} + \frac{1}{2}\sqrt{\mathcal{F}^2 + \frac{C_2^2 I_R^2 \omega_Z^2}{4 I_L^4}}} \quad (3a)$$

$$\omega_2 = -\frac{I_R \omega_Z}{2 I_L} - \sqrt{\frac{\mathcal{F}}{2} + \frac{1}{2}\sqrt{\mathcal{F}^2 + \frac{C_2^2 I_R^2 \omega_Z^2}{4 I_L^4}}} \quad (3b)$$

The damping coefficients may then be computed according to

$$D_1 = \frac{C_2}{2 I_L}\left(\frac{\omega_1}{\omega_1 + \frac{I_R \omega_Z}{2 I_L}}\right) \quad (4a)$$

$$D_2 = \frac{C_2}{2 I_L}\left(\frac{\omega_2}{\omega_2 + \frac{I_R \omega_Z}{2 I_L}}\right) \quad (4b)$$

The initial amplitudes and the phase angles are determined by the initial values of pitch angle, pitch rate, yaw angle and yaw rate. Let α_{X0} be the value of the yaw angle, Ω_{X0} the yaw rate, α_{Y0} the pitch angle and Ω_{Y0} the pitch rate at time equal to zero; then

$$A_1 \sin\varphi_1 = \frac{\left[\begin{array}{l}\Omega_{X0}(D_1 - D_2) + \Omega_{Y0}(\omega_1 - \omega_2) \\ + \alpha_{X0}(D_1 D_2 + \omega_1\omega_2 - D_2^2 - \omega_2^2) \\ + \alpha_{Y0}(\omega_1 D_2 - \omega_2 D_1)\end{array}\right]}{2(D_1 D_2 + \omega_1\omega_2) - D_1^2 - D_2^2 - \omega_1^2 - \omega_2^2}$$

$$A_2 \cos\varphi_2 = \alpha_{Y0} - A_1 \cos\varphi_1$$

$$A_2 \sin\varphi_2 = \alpha_{X0} - A_1 \sin\varphi_1$$

$$A_1 \cos\varphi_1 = \frac{\left[\begin{array}{l}\Omega_{X0}(\omega_2 - \omega_1) + \Omega_{Y0}(D_1 - D_2) \\ + \alpha_{X0}(\omega_2 D_1 - \omega_1 D_2) \\ + \alpha_{Y0}(\omega_1\omega_2 + D_1 D_2 - \omega_2^2 - D_2^2)\end{array}\right]}{2(D_1 D_2 + \omega_1\omega_2) - D_1^2 - D_2^2 - \omega_1^2 - \omega_2^2}$$

From these intermediate forms we obtain

*The phenomenon we have been referring to as inertial coupling is often called "pitch-roll coupling" by professional engineers. This is physically imprecise, however: pitch is coupled to yaw by the presence of roll, but roll is inertially coupled neither to pitch nor to yaw. We shall avoid this colloquialism and continue to use the term "inertial coupling."

(5a) $A_1 = \sqrt{(A_1 \sin \varphi_1)^2 + (A_1 \cos \varphi_1)^2}$

(5b) $A_2 = \sqrt{(A_2 \sin \varphi_2)^2 + (A_2 \cos \varphi_2)^2}$

(6a) $\varphi_1 = \text{ARCTAN} \left(\frac{A_1 \sin \varphi_1}{A_1 \cos \varphi_1}\right)$

(6b) $\varphi_2 = \text{ARCTAN} \left(\frac{A_2 \sin \varphi_2}{A_2 \cos \varphi_2}\right)$

The above solution describes pitching and yawing motions which are both sums of two different exponentially damped sinusoids. The appearance of the motion is generally quite complicated. The slower mode sets the basic pattern: the rocket's nose describes an inward spiral for stable motion, an outward spiral for unstable motion, a circle of constant radius for neutral stability. The mode with the faster angular frequency may impose intricate secondary motions called "nutations" if it is sufficiently fast and its amplitude is small. For statically stable rockets (corrective moment coefficient positive) the angular frequency of the fast mode will be opposite in sign to the roll rate, while the algebraic sign of the slow mode will be identical to that of the roll rate. The damping coefficients will both be positive, as both modes decay exponentially with time. The fast mode decays more rapidly than a decoupled oscillation with the same values of C_1, C_2, and I_L, while the slow mode decays less rapidly than such a decoupled oscillation. Since, as a practical matter, the slow mode will be the most important part of the oscillation after sufficient time has elapsed, inertial coupling serves to reduce the effectiveness of damping. It does, however, force the yawing and pitching motions to be oscillatory in nature regardless of the value of the damping moment coefficient C_2 and in this respect improves the dynamic behavior of an otherwise overdamped rocket.

In the limiting case of zero damping it may be seen that both D_1 and D_2 become zero; as in the decoupled case, the oscillations do not subside but persist indefinitely. Figure 2 shows a representative case of this behavior. Because true alignment with the intended flight path is not regained, such vanishingly slight damping would be an unfavorable characteristic, just as it was for decoupled motion. Some damping is, of course, always present and the motion of Figure 2 is never literally observed. Figure 3 shows a representative characteristic response of a statically-stable model having a finite amount of damping. This is the kind of behaviour favorable to model rocket flight: the oscillations decrease as time goes on and true alignment is subsequently regained.

As the static stability becomes less the angular frequency and damping coefficient of the slow mode decrease in magnitude, both becoming zero in the limit of neutral static stabilty. For negative static stability (corrective moment coefficient negative) the algebraic sign of the slow mode's angular frequency becomes opposite to that of the roll rate and the slow mode's damping coefficient becomes negative – the behavior has become divergent. The inertially coupled characteristic response of a statically unstable rocket is shown in Figure 4.

We can see how the roll-coupled behavior of a rocket is related to its decoupled response by examining the properties of the coupled solution as the roll rate approaches zero. For cases in which $\frac{C_2^2}{4I_L^2} < \frac{C_1}{I_L}$ the approach of the roll rate toward zero causes the angular frequencies to assume the values

$$\omega_1 = +\sqrt{\frac{C_1}{I_L} - \frac{C_2^2}{4I_L^2}}$$

$$\omega_2 = -\sqrt{\frac{C_1}{I_L} - \frac{C_2^2}{4I_L^2}},$$

which are just the positive and negative of the angular frequency of underdamped, decoupled motion as given in equation 2 of Part I. D_1 and D_2 both approach the value $C_2/2I_L$ given in equation 3 of Part I. For those cases in which $\frac{C_2^2}{4I_L^2} \geq \frac{C_1}{I_L}$ the disappearance of the roll rate causes both angular frequencies to become zero and the damping coefficients to become indeterminate forms involving zero divided by itself. This behavior is in keeping with the fact that decoupled responses in this range of dynamic parameters are nonoscillatory (either critically damped or overdamped); the occurrence of indeterminate forms is our signal that a solution predicting sinusoidal motions becomes invalid for zero roll rate.

In the opposite limit – that of C_1 and C_2 becoming insignificant compared to the coupling factor $I_R \omega_a$ – we can recognize the force-free gyroscopic

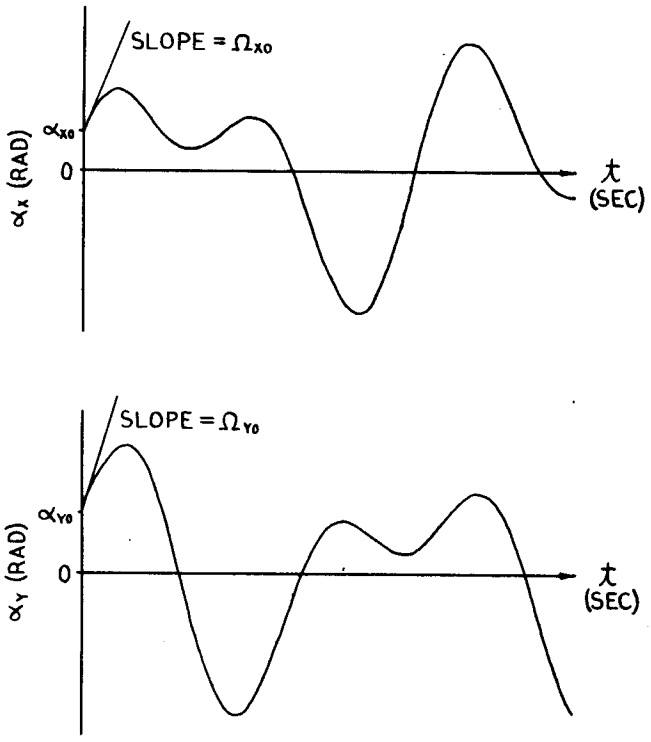

FIGURE 2. Undamped, inertially coupled homogeneous response to general initial conditions in pitch and yaw. The continuing sinusoidal oscillations of the fast mode are superposed upon those of the slow mode, producing "nutations".

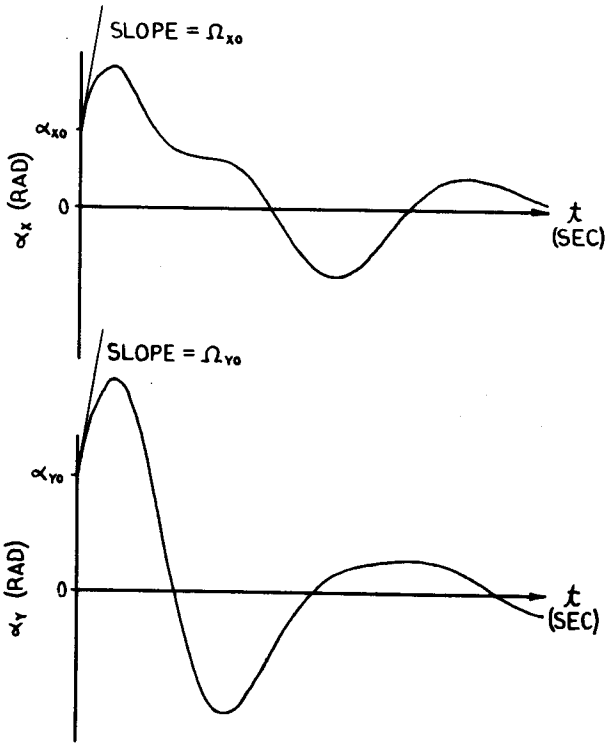

FIGURE 3. Coupled characteristic response of a representative model rocket having a finite amount of damping. The fast mode decays more rapidly than the slow mode.

precession mentioned in our discussion of inertial coupling. As the aerodynamic moment coefficients disappear the angular frequencies become

$$\omega_1 = 0$$

$$\omega_2 = -\frac{I_R \omega_R}{I_L}$$

and both damping coefficients become zero. This is the analytical description of the precession we pictured earlier: a steady, conical motion of the longitudinal axis about a cone axis which may, in general, have a direction different from that of the intended flight path.

Problem 2. Step-Response for Zero Initial Conditions

Recalling the discussion of step forcing given in Part I, we present the response of a spinning rocket to a step moment of value M_S applied at some time during a flight which has previously been straight and true. We choose to set the zero of our time scale to the time at which the step is applied and to solve the case in which the step forcing occurs entirely about the yaw (X) axis. This we can do without loss of generality, as the response to step forcing in pitch is precisely analogous to that in yaw.

The response to a step in yaw is given by

$$(7a)\quad \alpha_X = A_1 e^{-D_1 t} \sin(\omega_1 t + \varphi_1) + A_2 e^{-D_2 t} \sin(\omega_2 t + \varphi_2) + \frac{M_S}{C_1}$$

$$(7b)\quad \alpha_Y = A_1 e^{-D_1 t} \cos(\omega_1 t + \varphi_1) + A_2 e^{-D_2 t} \cos(\omega_2 t + \varphi_2)$$

where the angular frequencies and damping coefficients are governed by equations 3 and 4. The initial amplitudes and the phase angles must be computed using intermediate forms as follows:

$$A_1 \sin\varphi_1 = \frac{M_S}{C_1}\left[\frac{\omega_2^2 + D_2^2 - \omega_1\omega_2 - D_1 D_2}{2(D_1 D_2 + \omega_1\omega_2) - D_1^2 - D_2^2 - \omega_1^2 - \omega_2^2}\right]$$

$$A_1 \cos\varphi_1 = \frac{M_S}{C_1}\left[\frac{\omega_1 D_2 - \omega_2 D_1}{2(D_1 D_2 + \omega_1\omega_2) - D_1^2 - D_2^2 - \omega_1^2 - \omega_2^2}\right]$$

$$A_2 \sin\varphi_2 = -A_1 \sin\varphi_1 - \frac{M_S}{C_1}$$

$$A_2 \cos\varphi_2 = -A_1 \cos\varphi_1$$

from which we can obtain the results

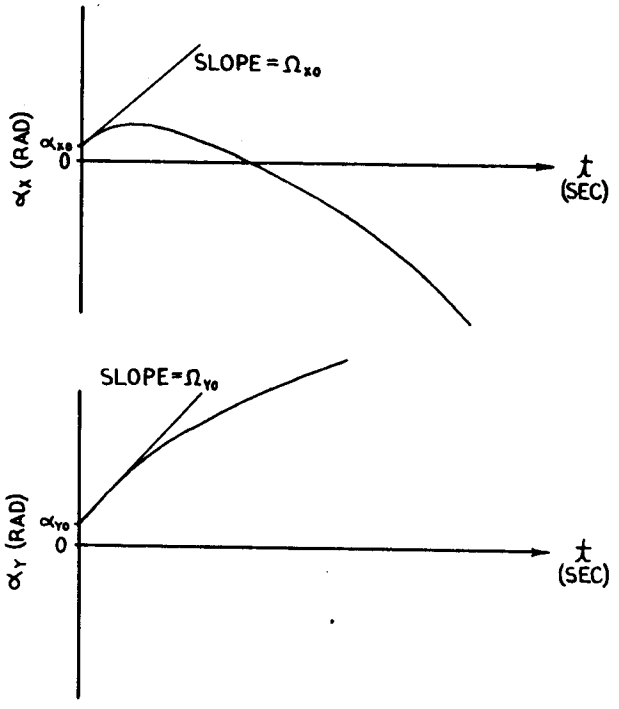

FIGURE 4. Coupled characteristic response of a statically unstable rocket. The fast mode decays, but the slow mode grows with time, producing divergent oscillations.

(8a) $$A_1 = \sqrt{(A_1 \sin\varphi_1)^2 + (A_1 \cos\varphi_1)^2}$$

(8b) $$A_2 = \sqrt{(A_2 \sin\varphi_2)^2 + (A_2 \cos\varphi_2)^2}$$

(9a) $$\varphi_1 = \text{ARCTAN}\left(\frac{A_1 \sin\varphi_1}{A_1 \cos\varphi_1}\right)$$

(9b) $$\varphi_2 = \text{ARCTAN}\left(\frac{A_2 \sin\varphi_2}{A_2 \cos\varphi_2}\right)$$

The motion predicted by these equations for a representative statically stable model with a reasonable damping moment coefficient is illustrated in Figure 5. As was the case for the decoupled response, we see that the yaw angle approaches a value of M_S/C_l radians after sufficient time has elapsed. The pitch angle, as in the homogeneous response, decays back to zero. The inverse dependence of the yaw angle on the corrective moment coefficient makes a large value of C_l desirable, confirming our conclusion of Part I. The reader can by now visualize the divergent sinusoidal motion associated with an unstable step-response and the continuing oscillations resulting from an absence of damping; we need not, therefore, illustrate these cases.

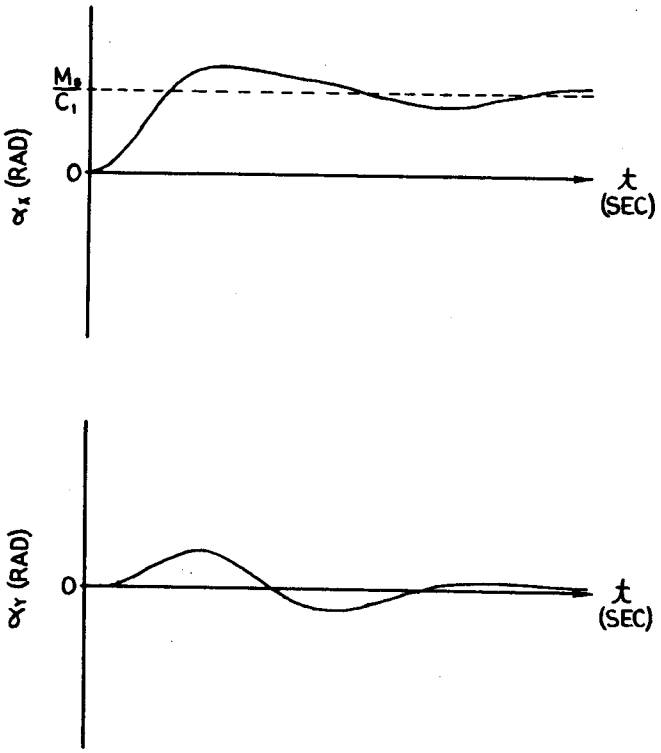

FIGURE 5. Inertially coupled step-response of a representative model rocket.

Problem 3. Impulse-Response for Zero Initial Conditions

Returning now to the concept of impulsive forcing presented in Part I, we shall write down the response of a spinning model rocket to an impulsive input of strength H in yaw under the assumption that the rocket in question has been flying straight and true prior to encountering the impulse at some time which we shall consider the zero of our time scale. Under these conditions the impulse-response is described by the equations

(10a) $$\alpha_X = A\left[e^{-D_1 t}\sin(\omega_1 t + \varphi) - e^{-D_2 t}\sin(\omega_2 t + \varphi)\right]$$

(10b) $$\alpha_Y = A\left[e^{-D_1 t}\cos(\omega_1 t + \varphi) - e^{-D_2 t}\cos(\omega_2 t + \varphi)\right]$$

where, again, the angular frequencies and damping coefficients are given by equations 3 and 4. The intermediate functions for determining the initial amplitude and the phase angle are

$$A\sin\varphi = \frac{H(D_1 - D_2)}{I_L\left[2(D_1 D_2 + \omega_1\omega_2) - D_1^2 - D_2^2 - \omega_1^2 - \omega_2^2\right]}$$

$$A\cos\varphi = \frac{H(\omega_2 - \omega_1)}{I_L\left[2(D_1 D_2 + \omega_1\omega_2) - D_1^2 - D_2^2 - \omega_1^2 - \omega_2^2\right]}$$

From these we can derive the relations

(11) $$A = \sqrt{(A\sin\varphi)^2 + (A\cos\varphi)^2}$$

(12) $$\varphi = \text{ARCTAN}\left(\frac{D_1 - D_2}{\omega_2 - \omega_1}\right)$$

The impulse-response of a typical model rocket is shown in Figure 6, in which it can be seen that the effect of the impulsive input is to cause a yaw rate equal to H/I_L to appear instantaneously at time equal to zero. The pitching and yawing motions of statically stable rockets thereafter increase to a maximum value, finally decaying again to zero. Although the equations for the maximum deflections are too involved to be written explicitly, it is evident that the severity of the impulse-response is inversely proportional to the rocket's longitudinal moment of inertia, and that consequently a large value of I_L is a desirable property in a model. This result reaffirms another of our conclusions from Part I.

Problem 4. Steady-State Response to Sinusoidal Forcing at the Roll Rate

As any rocketeer knows, all model rockets are subject to some slight configurational asymmetries and misalignments. These may arise during flight from such causes as minor structural failure or deflection, unintentional deflection of control surfaces, or canting of the rocket exhause due to imperfections in the motor, or they may be built into the model in the form of slightly misaligned fins or motor mounts. In Part I we stated that such things produce step disturbances, which is true as far as it goes; vehicle imperfections of this nature do indeed result in step forcing for rockets whose roll rate is zero. If our hypothetical rocket should acquire a roll rate, however, the source of the disturbing moment will rotate with the rocket and result in disturbing moments of the form

$$M_X = A_f \sin\omega_z t$$

$$M_Y = A_f \cos\omega_z t$$

This is seen to be a special variety of constant-amplitude sinusoidal forcing which occurs at an angular fre-

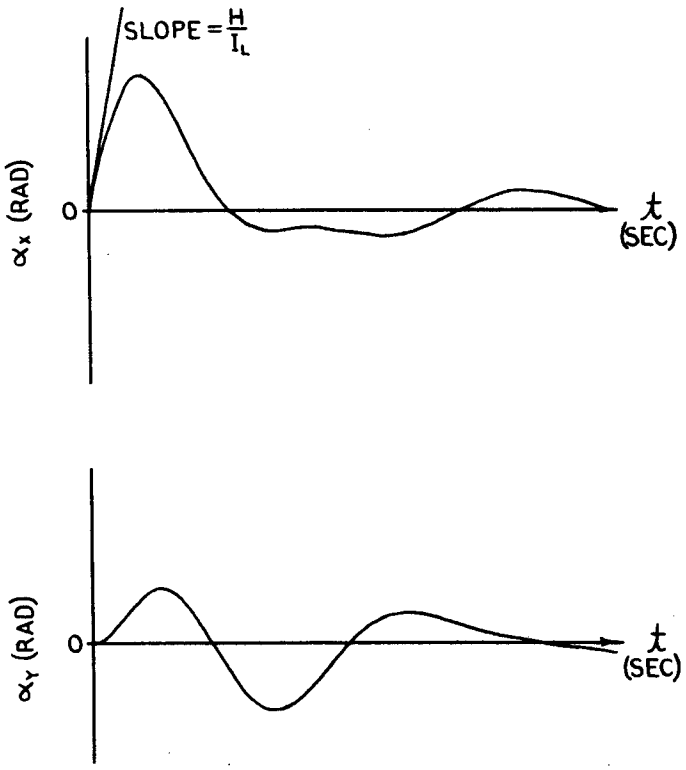

FIGURE 6. Coupled impulse-response of a representative model rocket.

quency equal to the roll rate of the rocket. As it is by far the most common, as well as the most important, oscillatory disturbance encountered by spinning rockets, it is the only one we shall discuss.

A disturbance of this type produces a sinusoidal response of constant amplitude in which the pitching and yawing motions are described by the equations

$$\alpha_x = A_r \sin(\omega_z t + \varphi) \tag{13a}$$

$$\alpha_y = A_r \cos(\omega_z t + \varphi) \tag{13b}$$

The response has an angular frequency equal to the roll rate, but its amplitude is different and it is "out of phase" with the disturbance by φ radians. The form of this motion is seen to be analogous to that of the decoupled frequency-response discussed in Part I, and its properties are studied in the same manner: by computing the dependence of the amplitude and phase angle of the response on the frequency of the disturbance. The response amplitude is given by

$$A_r = \frac{A_f}{\sqrt{[\omega_z^2(I_L+I_R)-C_1]^2 + C_2^2\omega_z^2}} \tag{14}$$

and the phase angle by

$$\varphi = \text{ARCTAN}\left[\frac{C_2\omega_z}{\omega_z^2(I_L+I_R) - C_1}\right] \tag{15}$$

These relations are similar to equations 34 and 35 of Part I, with the exception that the longitudinal moment of inertia is replaced by the sum of the longitudinal and radial moments of inertia. This similarity permits us to define a "coupled damping ratio" by

$$\zeta_c = \frac{C_2}{2\sqrt{C_1(I_L+I_R)}} \tag{16}$$

and a "coupled natural angular frequency" ω_{mc} by

$$\omega_{mc} = \sqrt{\frac{C_1}{I_L+I_R}} \tag{17}$$

Unlike the corresponding forms for decoupled motion, both these functions are complete artificialities; there exists neither a single natural frequency nor a unique damping ratio for inertially coupled motion, as we have shown in problem 1. The quantities defined by equations 16 and 17 do, however, greatly facilitate the frequency-response analysis of coupled motion. We can now define a coupled frequency ratio β_c by

$$\beta_c = \frac{\omega_z}{\omega_{mc}} \tag{18}$$

and, if we write the amplitude ratio of the response to the forcing function as

$$AR_c = \frac{A_r}{A_f} \tag{19}$$

we can obtain the convenient forms

$$AR_c = \frac{1}{C_1\sqrt{(\beta_c^2-1)^2 + (2\zeta_c\beta_c)^2}} \tag{20}$$

and

$$\varphi = \text{ARCTAN}\left[\frac{2\zeta_c\beta_c}{\beta_c^2-1}\right] \tag{21}$$

which are entirely analogous to equations 38 and 39 of Part I. Graphs of AR_c and φ as a function of β_c for several values of ζ_c are presented in Figures 7 and 8.

For values of $\zeta_c < .7071$ there exists a range of frequencies over which AR_c is greater than $1/C_1$ and a peak in AR_c at some value of β_c less than 1.0. This "resonance peak" is associated with a roll rate of

$$\omega_{z\,RES} = \omega_{mc}\sqrt{1-2\zeta_c^2} \tag{22}$$

and has a magnitude of

$$AR_{c\,RES} = \frac{1}{2C_1\zeta_c\sqrt{1-\zeta_c^2}} \tag{23}$$

As in the case of decoupled motion, too little damping can cause dangerously violent motions to result from even the slightest disturbance. As the damping increases the height of the resonance peak decreases toward $1/C_1$ and the resonant frequency toward zero, these values being reached at $\zeta_c = .7071$. Further increases in damping destroy the resonant behavior altogether and equations 22 and 23 become invalid.

For a given value of ζ_c the severity of the response can be lessened by increasing the value of C_1. The solution of equation 23 also points out the desirability, in statically-stable rockets,

FIGURE 7. The dependence of coupled amplitude ratio upon coupled frequency ratio for spinning rockets having various coupled damping ratios, showing the resonant behavior of those whose coupled damping ratios are less than .7071. For damping greater than this value no resonance occurs.

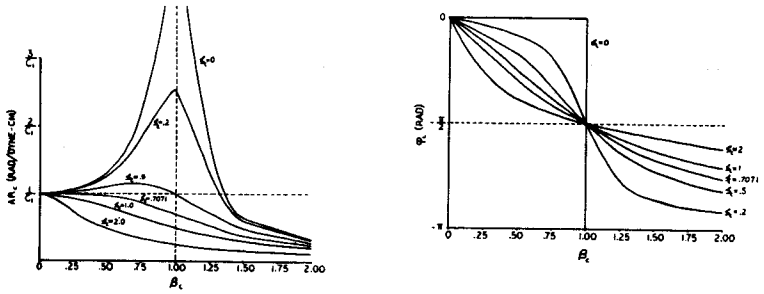

FIGURE 8. The dependence of phase angle upon coupled frequency ratio for spinning rockets having various coupled damping ratios.

of having a radial moment of inertia small compared to the longitudinal moment of inertia: if I_R is negligible compared to I_L the inertial coupling will not appreciably lessen the damping or the resonant frequency of the motion as compared with the decoupled case. The danger of an overly severe resonance is thereby minimized and we need not worry about encountering two distinct ranges of resonant behavior, depending on whether or not our rocket is spinning.

Roll Stabilization

It has long been known that inducing a roll rate in a rocket whose positive static stability margin is questionable improves its flight path and reduces the severity of its response to various disturbances. It is also common knowledge that the presence of an adequate spin rate will render the behavior of a statically unstable rocket acceptable for safe and predictable flight and it is therefore widely believed that the roll produces a condition of positive stability.

An examination of the results obtained in the four preceding problems, however, shows that roll actually stabilizes a rocket in the rigorous, physical sense only with respect to certain types of inputs: those connected with vehicle configurational or propulsive asymmetries. Such irregularities, we recall from Part I, are treated as step forcing for non-rolling rockets and produce angular deflections which grow exponentially with time in rockets whose static stability is negative. In problem 4 of this section we showed that step inputs of this nature are transformed into sinusoidal forcing when the rocket in question begins to roll. Inspection of equation 14 will reveal that a rocket whose corrective moment coefficient is negative exhibits a steady-state frequency-response whose amplitude is not only confined to values less than or equal to $1/C_{l_p}$, but which continues to decrease with increasing roll rate. In this respect a statically unstable rocket can be said to be stabilized by the presence of roll.

With respect to step inputs due to wind shears, however, and with respect to impulses due to launching and staging transients and momentary propulsive instabilities, the results of problems 2 and 3 of this article and the discussion of problem 1 show that spinning does not preduce stabilization; equations 3 and 4 indicate that one of the two sinusoidal modes of the response will grow with time. What the presence of the roll rate does do is to reduce the rate of growth of the motion's amplitude below that which would occur if the rocket were not rolling, and to reduce the initial amplitude of the response to a given disturbance below the value that would occur in a non-rolling rocket. As the roll rate is increased to very high values the effect of the aerodynamic moments becomes negligible and the rate of growth of the response becomes infinitesimal. Thus, in the strict physical sense, neutrally stable behavior is the best we can produce in response to inputs not due to vehicle or propulsive asymmetries – and this only by using a very fast roll rate, a very large radial moment of inertia, or both. As the oscillations need be restricted to small values only for the duration of the upward flight, however, the "stabilization" produced by spinning is adequate for engineering purposes provided that the product of the roll rate and radial moment of inertia is in great enough ratio to the magnitude of the (negative) corrective moment coefficient. A high spin rate and a large radial moment of inertia are thus both desirable characteristics for a statically unstable rocket which is to be roll-stabilized.

(Continued from page 4)

XR – 5C

gine or engines would still ignite the second stage engine, which would then fire down through the adapter igniting any live engines from the top. This results in internal fires and extensive damage to the booster and a power dive for the upper stages. An accompaning photograph shows an example of such a catastrophe. Also, even with sodium silicate fire-proofing, normal use would burn out the adapter in three launches.

To correct these problems, the adapter section was carefully redesigned. In the present design, two of the engines are blocked off completely. Only one engine is capable of igniting the second stage. If this engine does not ignite, one does not want the second stage to ignite anyway. If another engine does not ignite, it is impossible for the live engine to become ignited from the top. The one engine which is not blocked off is connected to the second stage by a short fire-proof tube. This tube is made as follows:

1. Cut out a strip of paper approximately 4" x 12" and wrap one end around a dowel 3/8" in diameter.

2. Prepare some epoxy glue and spread it out on the strip in a narrow band on the side of the paper strip which is just about to be rolled to the inside of the roll. Do not get any glue on the dowel.

3. Place the set-up on a hard surface and roll up the strip tightly, squeezing out the glue ahead of the roll.

4. Tape the roll so that it does not unwind, and let it set overnight. After the glue is set, remove the dowel and the tape.

The tube produced by this procedure is hard and extremely flame resistant. It can withstand the heat and fire of staging without noticeable deterioration. To use the tube, split a solid balsa adapter into two, carve out a channel in each half, as shown in the plans. Cut the tube to the appropriate lengths and glue them into the channel with liberal amounts of epoxy glue. Finally glue the halves of the adapter back together with white glue and let the assembly set overnight. While the glue is drying, stick each end of the adapter into body tube sections of appropriate sizes to hold the assembly together.

With the new type of adapter, the second stage should have about an inch of Jetex wick in its nozzle to ensure ignition.

The last remaining problem is ignition of the booster itself. I have had

Club Notes

The Model Rocket Space Club in Wheeling, West Virginia reports in the latest edition of their newsletter that their president and vice-president attended a meeting of the National Science Foundation of West Virginia. The meeting, on August 7 to 10, was held at Green Bank, West Virginia. This was followed by a 4 1/2 hour tour of the radio telescope installation at Green Bank.

The MIT Section of the National Association of Rocketry has announced its intention to hold its second annual technical convention in the early spring of 1969. The MIT convention, which has become a source of technological advancement for the hobby, thus joins the Steel City Section's Pittsburgh convention as an annual event.

Send your club newsletters, contest announcements and results, and other news items for this column to:
Club News Editor
Model Rocketry Magazine
P.O. Box 214
Boston, Mass., 02123

(XR-5C Continued)

best results using the three-pieces-of-Jetex-wick-and-one-igniter method, but this is an area which still needs study.

Computer calculations done at M.I.T. and elsewhere predict an apex of 2500 to 3000 feet with three C engines in the first stage, a C engine in the second stage and a B engine in the third stage. It would be interesting to see how this calculation compares to actual apex altitudes, but the third stage is nearly out of sight when it ignites (calculated altitude of third stage ignition: 1000 feet) and it is so far out of sight at apex that, until better tracking methods are developed, one can only guess at how high the third stage makes it. Even with a six foot long streamer the third stage is extremely difficult for recovery crews to locate on the way down and it is easily lost. The second stage is also very difficult to recover. Do not launch this rocket without an alert and experienced recovery crew. Station crews at points 1000 feet from the launch site in several directions. Then simply watch closely and good luck!

This picture was taken seconds after the first launch of the XR-5A. White areas on the right are snow. White areas on the left are smoke from the burning parts. An upper stage fin is visible in the upper left.